RL-TR-97-138
Final Technical Report
October 1997

DLMS OPTICAL MEMORIES

Hughes Research Laboratories

Wu, C.S., Dalton, L.R., and Efron, U.

DTIC QUALITY INSPECTED 4

APPROVED FOR PUBLIC RELEASE; DISTRIBUTION UNLIMITED.

19980209 071

Rome Laboratory
Air Force Materiel Command
Rome, New York

This report has been reviewed by the Rome Laboratory Public Affairs Office (PA) and is releasable to the National Technical Information Service (NTIS). At NTIS it will be releasable to the general public, including foreign nations.

RL-TR-97-138 has been reviewed and is approved for publication.

APPROVED: *Gary L. Sunada*

GARY L. SUNADA, 1Lt, USAF
Project Engineer

FOR THE DIRECTOR: *Frederick L. Berg*

FREDERICK L. BERG, Lt Col, USAF
Acting Director
Intelligence & Reconnaissance Directorate

REPORT DOCUMENTATION PAGE

*Form Approved
OMB No. 0704-0188*

1. AGENCY USE ONLY *(Leave blank)*	2. REPORT DATE	3. REPORT TYPE AND DATES COVERED
	Oct 97	Final May 95 - Feb 97

4. TITLE AND SUBTITLE

DLMS OPTICAL MEMORIES

6. AUTHOR(S)

Wu, C.S., Dalton, L.R., and Efron, U.

5. FUNDING NUMBERS

C - F30602-95-C-0133
PE - 62702F
PR - 4594
TA - 15
WU- P3

7. PERFORMING ORGANIZATION NAME(S) AND ADDRESS(ES)

Hughes Research Laboratories
3011 Malibu Canyon Road
Malibu, CA 90265

8. PERFORMING ORGANIZATION REPORT NUMBER

27457

9. SPONSORING/MONITORING AGENCY NAME(S) AND ADDRESS(ES)

Rome Laboratory/IRAP
32 Hangar Rd
Rome, NY 13441-4114

10. SPONSORING/MONITORING AGENCY REPORT NUMBER

RL-TR-97-138

11. SUPPLEMENTARY NOTES

Rome Laboratory Project Engineer: 1Lt Gary T. Sunada, IRAP, 315-330-2499

12a. DISTRIBUTION AVAILABILITY STATEMENT

Approved for public release; distribution unlimited.

12b. DISTRIBUTION CODE

NA

13. ABSTRACT *(Maximum 200 words)*

The concept of Dye-Labeled MicroSphere (DLMS)-based optical memory is based on the use of morphological resonances in microspheres to form a 3-D memory where two dimensions are spatial and the spectral frequency constitutes the third dimension. Following the successful feasibility demonstration of the Phase I concept, the second phase thrust was 1) improve dye material switching speed and near-IR sensitivity, 2) perform theoretical studies of the morphological resonance to estimate storage density, 3) perform a study to project DLMS-based system performance. In the area of material development and synthesis we have studied and demonstrated several methods of controlling the attachment or coupling of the chomophore molecules (dye material) to polystyrene microspheres. We also performed a systematic exploration of the production of other functionalized microspheres. In addition, we have synthesized a high-performance Thio-Indigo dye, characterized and evaluated its bi-stable characteristics. For theoretical studies we have developed a Mathematical package for Mie scattering from structures exhibiting the MDR effect. The study results indicated that a real storage density is worse than conventional optical disk. 3-D cubic packing of the microspheres would improve storage, but the large pixel size required is impractical. In order to exploit the high-efficiency dyes developed by this effort, we redirected the effort towards 2-D memory application. However, the result with Thio-Indigo and its derivatives show a relatively low spectral conversion rate, which is insufficient for optical memory applications.

14. SUBJECT TERMS

Optical memories, spectral holeburning, dye-labeled microsphere, morphological resonance

15. NUMBER OF PAGES

76

16. PRICE CODE

17. SECURITY CLASSIFICATION OF REPORT	18. SECURITY CLASSIFICATION OF THIS PAGE	19. SECURITY CLASSIFICATION OF ABSTRACT	20. LIMITATION OF ABSTRACT
UNCLASSIFIED	UNCLASSIFIED	UNCLASSIFIED	UL

CONTENTS

ILLUSTRATIONS

ILLUSTRATIONS (Continued)

Page

ILLUSTRATIONS (Continued)

TABLES

Section 1
INTRODUCTION

Physical limitations such as spatial resolution, signal-to-noise ratio and cross talk, control the current performance of 2-D memories (both magnetic and optical). Present limitations are: (a) relatively low storage density ($\approx 10^8$ bits/cm^2), (b) low throughput rate ($\sim 10^6$ bits/sec) and (c) slow access time ($> 10^{-3}$ sec). However, as information technology plays an increasingly important role in both military and commercial applications, more powerful computing power demands ever larger data storage capacity. Naturally, the data transfer rate and data access time of large-capacity data storage devices ought to be significantly improved so they will not become bottlenecks to the system. For example, next generation supercomputers and real time data acquisition/processing and pattern recognition systems will require higher storage density ($\times 10^4$), a higher throughput rate ($\times 10^3$) and faster access time ($\times 10^{-3}$). Yet despite intensive research efforts devoted to squeezing more capacity into the device, current 2-D optical storage technology may reach its theoretical limit of storage density, 10^8 bits/cm^2, by the end of this century. In addition, parallel I/O and parallel processing, which can alleviate the throughput bottleneck, are rather difficult to implement in the current 2-D memory systems. Hence, to meet future needs for extremely high-density data storage devices, innovative memory principles are being eagerly explored.

The most natural approach to improve storage density is to extend the 2-D storage to multi-dimensional domains. Holographic data storage and two-photon data storage represent typical examples of packing data into a 3-D (X, Y and Z spatial dimensions) volume space. Another elegant approach relies on the introduction of the optical frequency as the additional storage dimension (wavelength multiplexing). Digital information may be encoded into the optical frequency domain and densely packed at the same spatial spot on the storage medium. While the Z dimension is usually limited by the optical depth of field, the large optical frequency dimension ($\sim 10^{14}$ Hz) can provide an extremely large multiplexing capability to significantly enhance data storage density.

The persistent spectral hole-burning (PSHB) effect in suitable materials was suggested to provide the frequency selectivity required for the wavelength multiplexing approach. Resulting from strain-induced frequency shifts on the atomic or molecular resonance, homogeneous absorption lines of optically active centers are inhomogeneously broadened. Each individual homogeneous line within the inhomogeneously broadened band may be

selectively excited by a narrow-band optical excitation, on the condition that the excitation frequency is in resonance with the transition frequency of the particular homogeneous line.

The number of spectral holes which may be independently excited depends on the ratio of the inhomogeneous to homogeneous linewidth, the frequency multiplexing factor.

In principle, the frequency multiplexing factor can be as large as 10^6 if ultralow cryogenic temperature is permissible. Since thermal energy can activate the transition and significantly broaden the homogeneous linewidth, it is generally necessary to maintain the operation in a cryogenic environment. An estimation has indicated that the frequency multiplexing factor may reach ~400 at 77K and that it will quickly drop to ~20 at room temperature. Although low temperature (~4K) may be reliably accomplished using commercially available cryocoolers, this requirement may prove to be too stringent for the commercial market. For practical high-density storage applications, it has even been suggested to pursue higher operation temperatures (for example, room temperature) at the expense of lower multiplexing factors.

The recognition of the need for high temperature spectral hole-burning has stimulated increasing research efforts in material development and physical configurations. For example, intensive studies have been devoted to development of room-temperature PSHB materials such as organic solutions, Sm^{2+}-doped crystals, and Sm^{2+}-doped glasses. In this research, two to three spectral holes were successfully burned into the samples and retrieved at room temperature. In addition, a new room-temperature PSHB mechanism has been proposed and observed in dye-labeled microparticles. Spectral hole-burning was also recently observed in sol-gel CdS quantum dots at room temperature.

For the first phase of this program we have developed a high dimensional 3-D/4-D Write/Erase/Read (W/E/R) optical memory system with parallel access capability allowing a fast data transfer rate. The Dye Labeled Micro Sphere (DLMS) erasable memory utilizes inherent Morphology Dependent Resonances (MDRs) of microspheres for the necessary wavelength selectivity. The sharp MDR homogeneous lines characterize the interaction of light with a high precision microsphere at ambient temperature. An inhomogeneous distribution of multiple narrow resonance lines, representing slight changes in the microsphere sizes, will result in a broad overlapped spectrum composed of the separate but slightly shifted resonances. As each individual resonance is defined mostly by the quality factor (Q-value) of the corresponding microsphere morphology, this arrangement will result in sharp homogeneous resonance lines inhomogeneously broadened at ambient temperature. These sharp resonances will correspond to frequency slots in the spectrum that can be individually encoded by the writing light. The data encoding is based on the direct interaction of writing photons with the electrons in bi-stable dye molecules to induce

a reversible photochromophores isomerization process. As the dye molecules are transformed to the encoded isomeric phase, they will be distinguished by a change in their chemical configuration resulting in a different spectral signature. Attaching these molecules to the surfaces of a high precision microsphere distribution allows the isomerization which occurs resonantly in only one particular microsphere morphology (within a specified spectral range). The writing process will eliminate the particular homogeneous resonance line from the inhomogeneous distribution and multiple images may be encoded and stored in the optical frequency domain. The use of a relatively broad spectrum of the bi-stable dye permits us to "burn" multiple narrow-band spectral holes in the system, thus achieving a large magnitude wavelength multiplexing factor for high-density data storage. Furthermore, the introduction of the bi-stable dyes also opens the door to satisfying the need for erasable memory systems. A schematic of the DLMS memory system is shown in Figure 1-1.

To achieve room-temperature spectral hole-burning using dye-labeled polymer microspheres, the following materials issues have been addressed in our Phase I research: (1) polymer microspheres of dimensions ranging from several hundred nanometers to 20 mm were synthesized with good control of the distribution of microsphere sizes and the chemical contamination of the sphere surfaces; (2) appropriate photochromophores which permit the desired optical changes to be effected, read or detected, and erased; and (3) the attachment of the dye to the microspheres in a controlled manner so that the appropriate index of refraction coating is greater on the microsphere surface. During Phase I of this program we have demonstrated the feasibility of DLMS-based erasable memory operations. By showing the ability to read write and erase at multiple wavelengths, a typical example is shown in Figure 1-2.

3
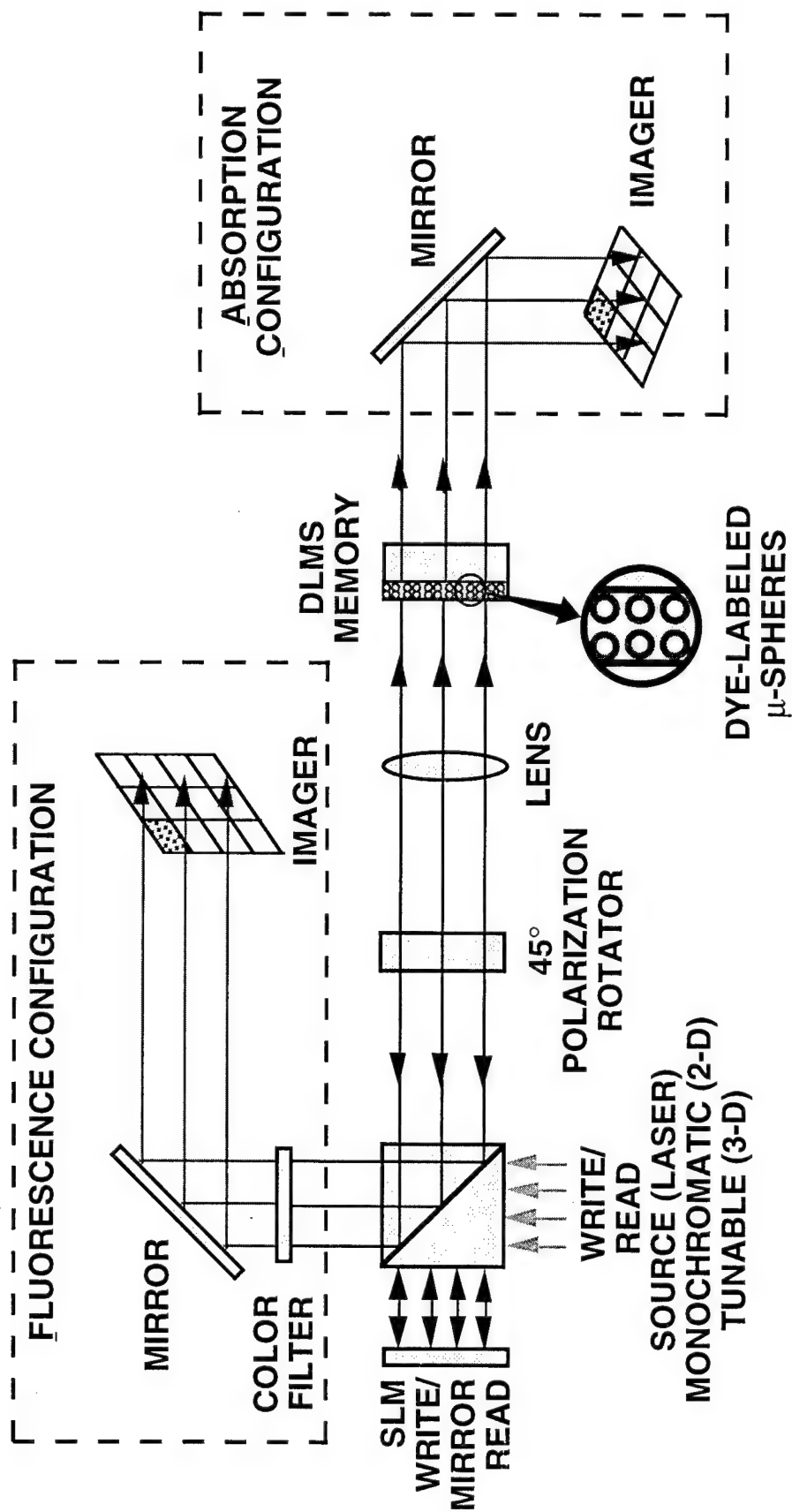
Figure 1-1. Schematics of the DLMS Optical Memory System

4
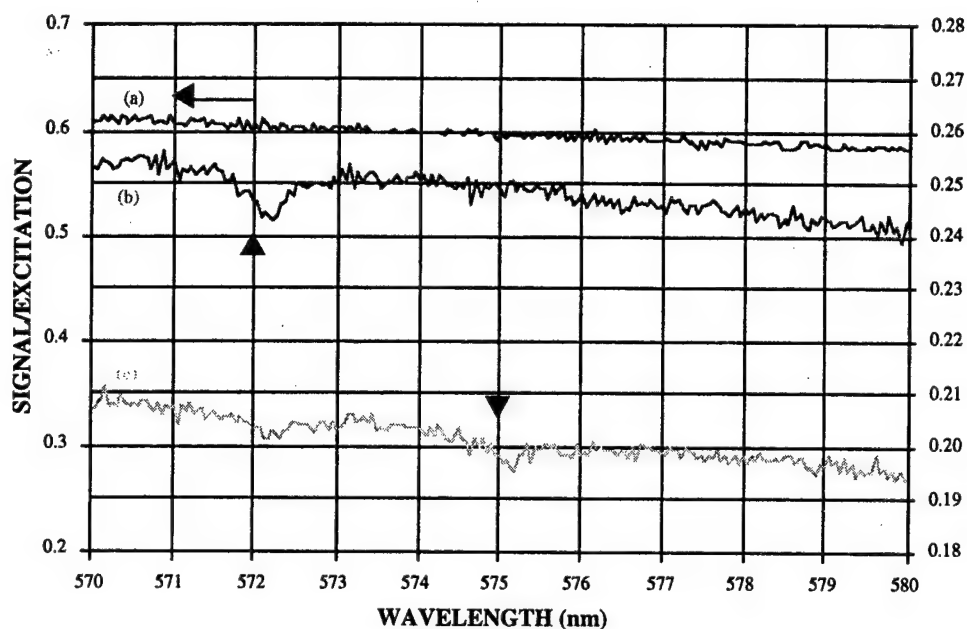
Figure 1-2 (a). Spectral hole formation, erasure, and hole-rewriting in a DLMS sample. *Two spectral holes were burned into the sample: curve (a) is the spectrum taken from the fresh sample before the spectral holes were burned, curve (b) shows the first spectral hole after a two-minute hole-burning at 572 nm, curve (c) shows the second spectral hole after a one-minute hole-burning at 575 nm (note both holes are recognizable).*
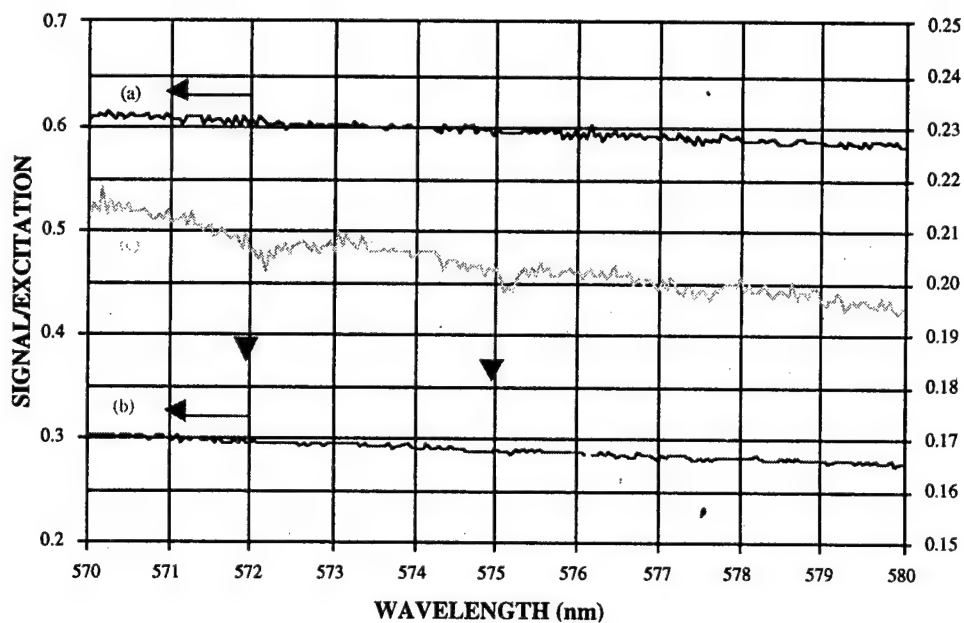
Figure 1-2 (b). Optical erasure of the burned spectral holes. *After two spectral holes were burned into the samples, optical erasure was attempted on two samples. Sample A [see (A) above] was submitted to 10 minutes' exposure; Sample B [see (B)], to 20. Here curve (b) is the spectrum right after the holes formation and being kept in the dark for 20 minutes, and curve (c) is the spectrum measured after the UV erasure.*
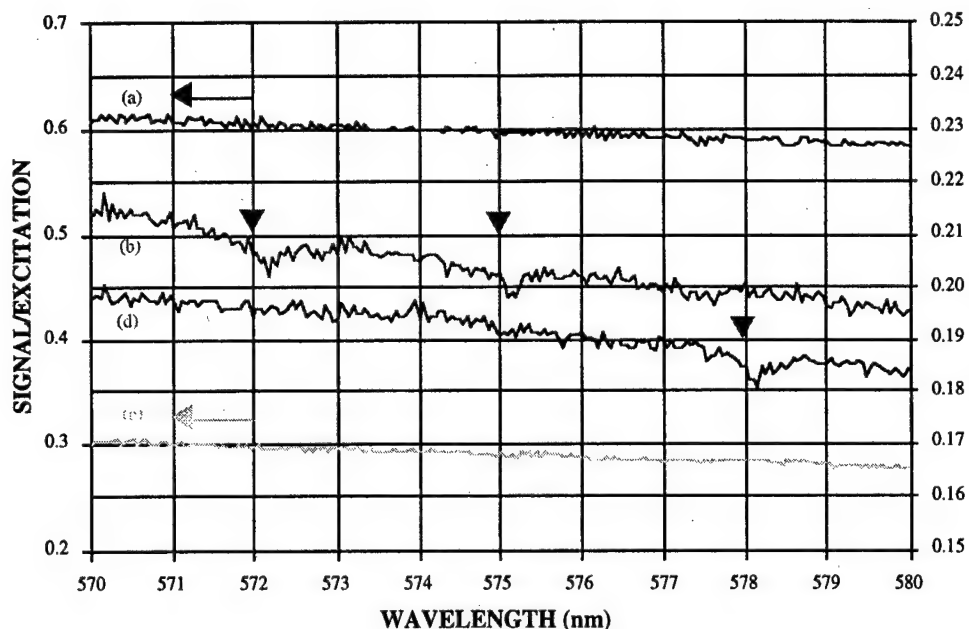
Figure 1-2 (c). Rewriting of spectral hole in a freshly-erased sample (Sample B). *Two spectral holes were burned into the sample: curve (a) is the spectrum taken from the fresh sample before the spectral holes were burned, curve (b) shows the two previously burned spectral holes, curve (c) shows the spectrum after the optical erasure, and curve (d) shows the newly formed spectral hole after a one-minute hole-burning at 578 nm.*

The thrust of the second phase of the DLMS project was in 3 main directions:

1. Improve the dye materials in terms of their switching speeds and near-IR sensitivity.

2. Perform theoretical studies of the Morphological Resonance to acquire a good understanding of the effect, and allow realistic estimates of storage density to be extracted.

3. Perform a study to project the performance of a DLMS-based system.

In the area of material development and synthesis we have studied and demonstrated several methods of controlling the attachment or coupling of the chromophore molecules (the dye material) to the polystyrene microspheres. In order to achieve chromophore attachment a variety of polar and hydrogen bonding solvents and mixed solvent systems were explored. We were ultimately able to achieve chromophore coupling and have produced several samples. However, due to a variety of problems associated with bead aggregation and disruption that occurred during the fabrication processes, these materials were found to be unacceptable.

We subsequently began a systematic exploration of the production of other functionalized polystyrene microspheres incorporating amine groups, sulfonyl chloride, and other functionalities. Fortunately, reduced intermolecular interactions were observed

for these other chromophores but achieving a high degree of surface functionalization without compromising crosslink density remained a problem.

Ultimately, we were able to achieve essentially monolayer coverage of the polymer microsphere surface with high crosslink density. Samples obtained near the end of the contract period have essentially approached monolayer coverage without disruption of microsphere structure.

Finally in this area of material development we have synthesized a high performance Thio-Indigo dye, characterized it and performed an evaluation of its bi-stability characteristics for the DLMS optical memory application.

In the area of theoretical studies we have developed a Mathematica package for Mie scattering from structures exhibiting the MDR effect. we then have developed tools to estimate the data storage density (under the optimal conditions) and used the results for the system study. Another thrust of the theoretical effort was to study the effect of microsphere size as well as the effects of material refractive index and the absorption coefficient on the Quality Q-factor. We then proceeded to model the DLMS as single-layer coated microspheres and study the effects of layer thickness and layer refractive index on the MDR phenomenon. For layer thickness more than 20% of the microsphere diameter, the effective MDR was found to be qualitatively similar to the homogeneous microsphere made of the same material. The conclusion is therefore that the simulation of homogeneous microspheres may be applied to such layer-coated samples.

Next we studied the effects of lateral coupling on the Q factor. The main concern was the effect of such coupling on the microsphere packaging. Only qualitative arguments were used in this study and no physical simulation tools were developed.

Finally, we have used the results of the theoretical analysis to perform a performance analysis of the DLMS Optical Memory system.

In principle the DLMS does allow a reasonable multiplexing factor (MF) to microspheres with well-controlled size distribution, although the MF is not as large as we anticipated. Larger MF may be achieved for a microsphere distribution with a large average size, a resonance condition matched to the first order MDR, and a negligible Q-loss caused by material absorption. An important criterion from the system standpoint is whether the areal storage density (bit/μm^2) of the system outperforms the conventional optical disk (≈ 1 bit/μm^2).The results of the study indicated that the areal storage density is actually lower than that of a conventional optical disk. This areal storage density can be improved by packing all microspheres in a 3-D cubic format. However, the gain can be realized only if the MF is large, which implies that large areal size (to achieve large Q) is needed. Naturally, it also implies that a large pixel size, on the order of $(MF)^{1/3} \times (2a)$, where a is the

microsphere diameter, is required to accommodate so many microspheres. Unfortunately, it will not be practical to have 2-D page-mode operation with large pixel size.

Since we have reached the conclusion the DLMS concept, although viable, will not be competitive compared to other 3-D type structures, we have redirected the effort in the last few months of the program. The new direction was aimed at exploiting some of the high-efficiency dyes developed, to result in an efficient dye for a 2-D memory application.

However the results with Thio-Indigo and its derivatives showed a relatively low spectral conversion rate which, at this point will not be sufficient for Optical memory applications.

Section 2
MATERIAL DEVELOPMENT

Our initial research focused on uncontrolled (multi-layer) coupling of photochromic molecules to the surface of polystyrene microspheres. In the present research, our focus turned to controlled single layer and step-by-step controlled layer deposition (coupling) of polystyrene microspheres to the surface polystyrene beads and to the development of new photochromic materials.

2.1 SYNTHESIS OF FUNCTIONALIZED MICROSPHERES

Let us first review our efforts on controlled coupling of chromophores to the surface of polystyrene microspheres. The essential issue here is the controlled functionalization of the surface of polymer microspheres in a manner which permits controlled chemical reactions to be carried out. This was a difficult and unexplored area of chemical research when we approached the problem and we recognized at the outset that we would face several serious problems. The central problem which must be overcome is that controlled organic reactions typically involve the use of specific organic solvents but polystyrene microspheres are disrupted by such solvents unless very high levels of crosslinking of the polystyrene chains are achieved. Thus, we faced the issue of developing new synthetic protocols for high crosslink density polystyrene microspheres with a high level of surface functionalization of -OH, $-NH_3$, -S(=O)Cl, etc. groups and of exploring the use of new solvent systems in the subsequent coupling reactions involving chromophore-polymer microsphere coupling.

Two routes were originally proposed to achieve controlled coupling of chromophores to microspheres. The first involved modification of the well-known [styrene + divinylbenzene $\rightarrow$ polystyrene microspheres (PSMS)] (see Figures 2-1 to 2-3) emulsion polymerization reaction by introducing a third reactant consisting of a chemical functionality attached to the para position of styrene.

9
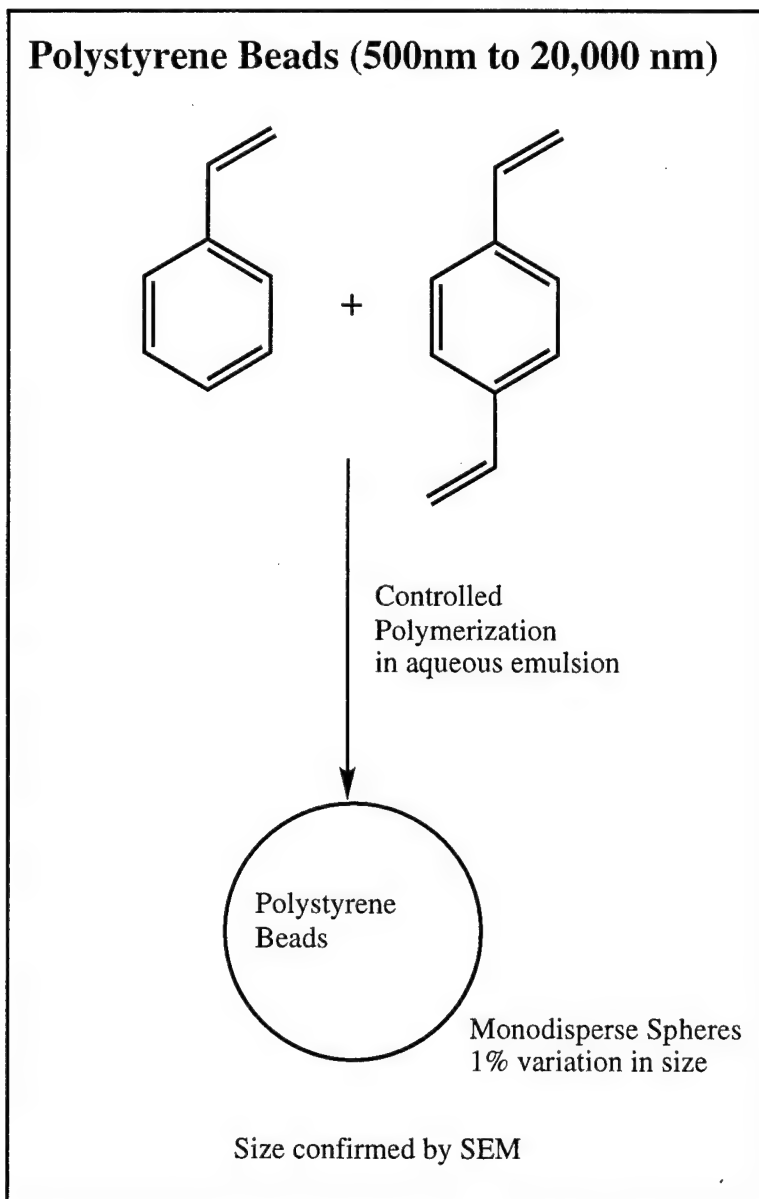
Fig 2-1 Formation of polystyrene microspheres of well-controlled size distribution by emulsion polymerization. *The parent styrene can be functionalized to produce functionalized, crosslinked microspheres.*
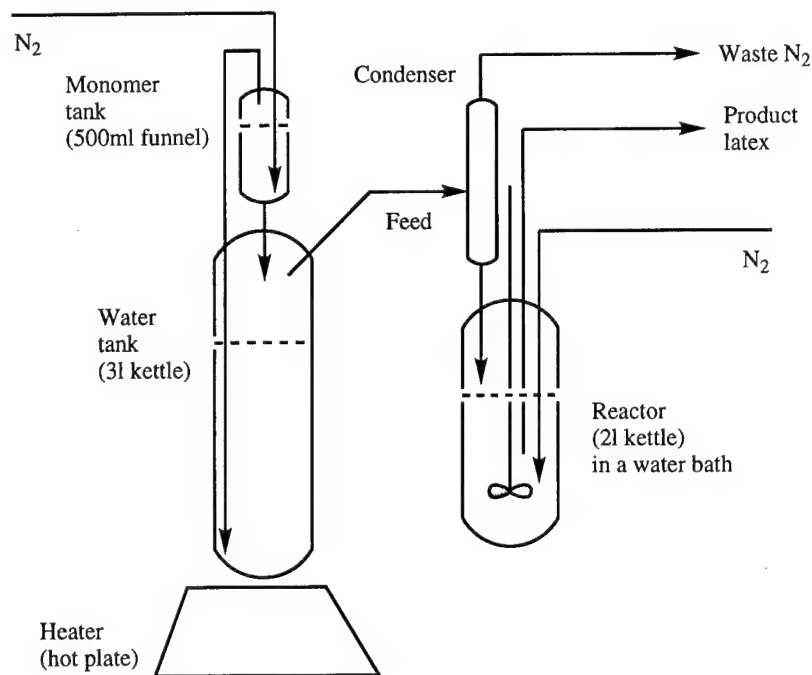
Figure 2-2. Experimental equipment for continuous emulsion polymerization-formation of polystyrene microspheres.

SEM of Polystyrene Microspheres (400-600 nm)
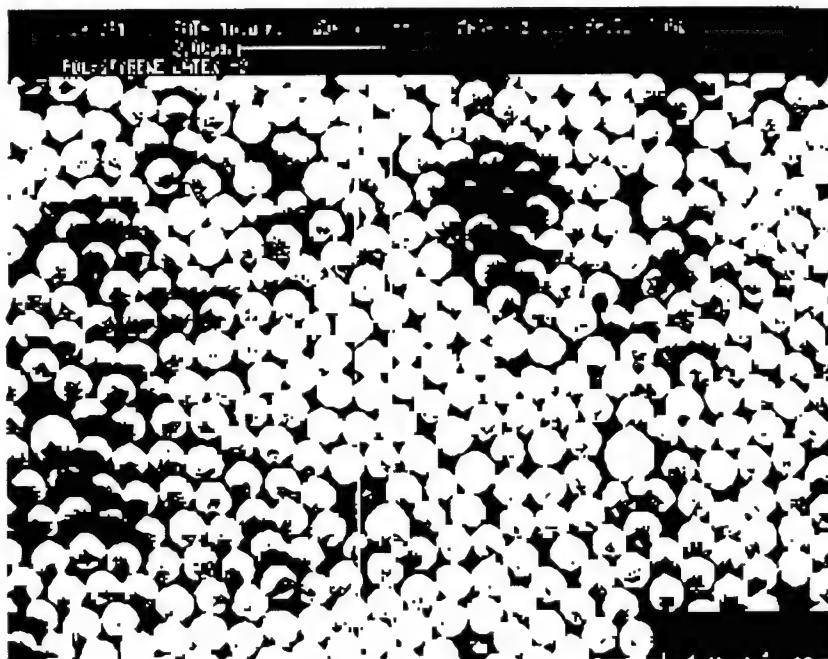
Figure 2-3. Scanning electron micrograph of polystyrene microspheres prepared via Figures 2-1 and 2-2.

The functionality must be chosen to be the one used in subsequent coupling of the chromophore or must be a functionality which can be readily converted to an appropriate coupling functionality. The functionality must not interfere with the desired polymerization and crosslinking reactions and the functionality must survive the emulsion polymerization reactions. Since we are interested in functionalities which undergo controlled condensation reactions to couple chromophores and polymer microspheres and since the polymerization and crosslinking (involving divinylbenzene) reactions are free radical reactions involving the vinyl functionality, the avoidance of functionality participation is well achieved. What is more difficult to achieve is a high level of functionality incorporation without reducing the crosslink density. The second approach is to functionalize the surface of preformed, high crosslink density polymer microspheres (see Figure 2-4). On the surface this might seem like a straight forward approach but in reality this is an unexplored area of chemistry.

Electrophilic Reactions of Polystyrene

$E = NO_2$, Cl, Br, R, CHO, COR, etc.
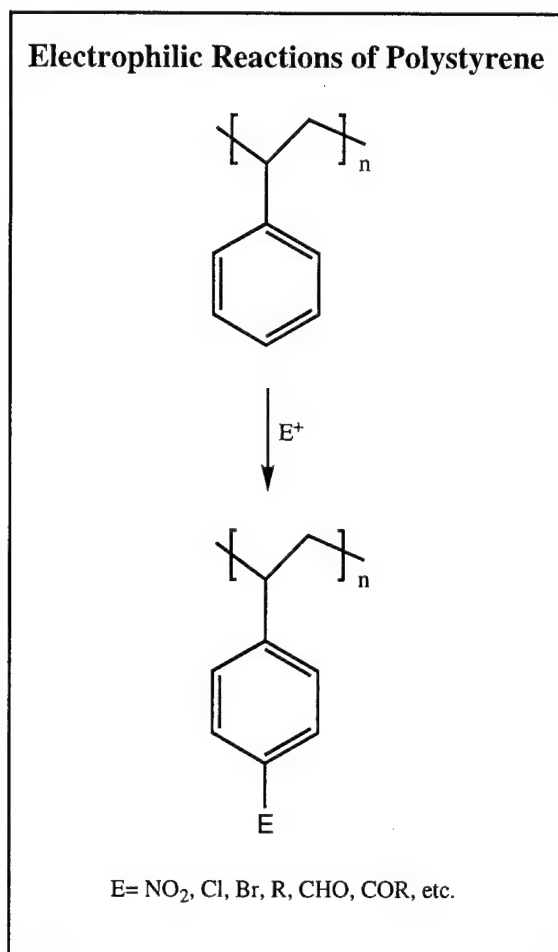
Figure 2-4. Generic examples of functionalization of polystyrene. *The reactions may be performed on the surfaces of polystyrene particles.*

The critical problem is that functionalizing polymer surfaces requires harsh reagents and solvent conditions that could easily disrupt polymer microsphere surfaces. Let us review our experiences with each of these approaches.

The first functionalization reaction following the first approach which we explored was the production hydroxylated surfaces by the following reaction:

styrene + divinylbenzene + p-hydroxylated styrene —> (PSMS)-(OH)$_x$
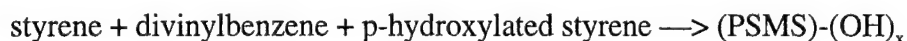
A critical problem is the difference in reactivity ratios of the various monomers. Numerous reactions were run systematically varying the ratios of monomers used in the reaction feed. Such studies revealed that it was impossible to simultaneously achieve both high surface functionalization and high crosslink density. However, an even more serious problem was identified for hydroxylated polystyrene microspheres and that was found to be a high level of intermolecular interaction (aggregation) driven by hydrogen bonding involving the hydroxyl groups of the functionalized microspheres. Only in hydrogen bonding solvents such as water could aggregation be avoided. To achieve chromophore attachment a variety of polar and hydrogen bonding solvents and mixed solvent systems were explored. We were ultimately able to achieve chromophore coupling and samples were delivered to Hughes for optical memory evaluation. However, due to a variety of problems associated with bead aggregation and disruption that occurred during the fabrication processes, these materials were found to be unacceptable. Because of the problems identified with the production of (PSMS)-(OH)$_x$ materials, the production of these materials was discontinued. In passing it should be noted that while such materials are not appropriate for optical memory applications such surface functionalized microspheres may have other applications as in catalyst supports and templates for sequential synthesis.

We subsequently began a systematic exploration of the production of other functionalized polystyrene microspheres incorporating amine groups, sulfonyl chloride, and other functionalities. Fortunately, reduced intermolecular interactions were observed for these other chromophores but achieving a high degree of surface functionalization without compromising crosslink density remained a problem. When crosslink density was too low, we were unable to identify a solvent system which permitted coupling of chromophores to polymer microspheres without disruption of the microsphere structure. Several samples were provided to Hughes which proved unacceptable because of perturbation of microsphere structures during the chromophore coupling reaction. Ultimately, we were able to achieve essentially monolayer coverage of the polymer microsphere surface with high crosslink density. Samples obtained near the end of the contract period may have essentially approached monolayer coverage without disruption of microsphere structure. However, concurrent theoretical analysis indicated that some of the degradation in morphological resonance quality factors observed with monolayer coverage was to be expected; thus, the observed poorer

optical memory response observed for microspheres with monolayer coverage likely reflected both synthetic and theoretically-predicted degradation in performance relatively to microspheres with thick chromophore coatings studied in the first contract period.

The second approach involved the post-fuctionalization of preformed polymer microspheres stabilized by high crosslink density. Here, we were able to realize a substantially more successful route to functionalized microspheres which can withstand the conditions of chromophore coupling reactions. The advantage of this approach is the original styrene (vinylbenzene) plus divinylbenzene (crosslinking reagent) reaction can be optimize to yield very high (20%) crosslink density. These highly stable microspheres were then functionalized subsequently.

Our first experiments focused on functionalizing preformed polystyrene microspheres with hydroxyl groups (see Figure 2-5). This effort was pursued concurrently with the modified emulsion polymerization approach discussed above.
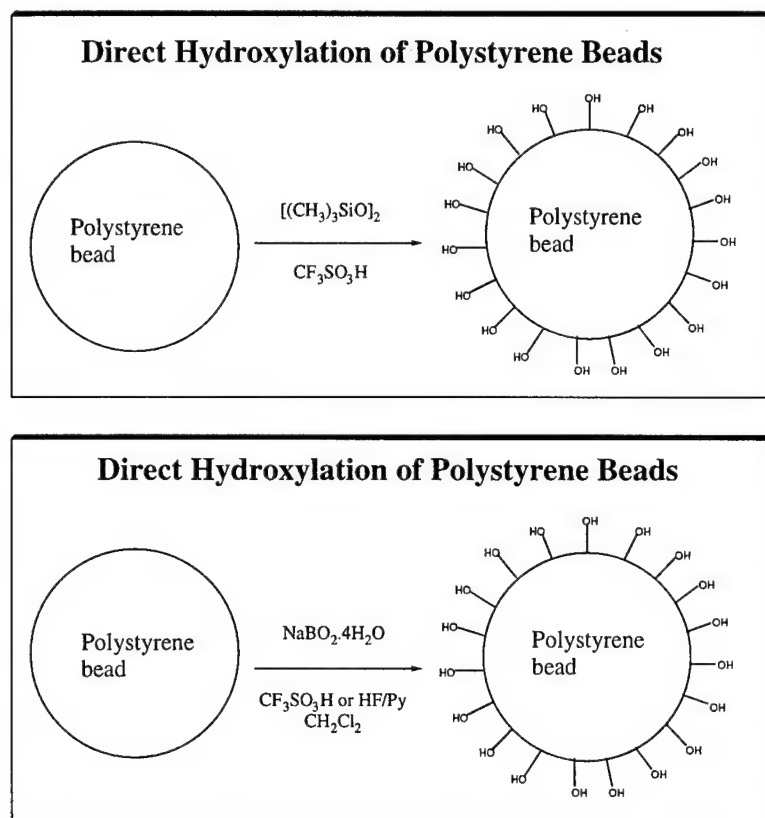
Figure 2-5. Two methods for the direct hydroxy surface functionalization of preformed polystyrene beads.

A variety of hydroxylation reaction conditions were investigated but the route which was found most satisfactory involved mild reaction conditions using hydrogen peroxide and a strong acid (the superacids made famous by our collaborator and Nobel Laureate, George A. Olah (Figures 2-6, 2-7, and 2-8). The hydroxylated polystyrene microspheres where characterized by SEM and by surface IR methods (see Figures 2-9, 2-10, and 2-11). Infrared spectroscopy clearly established a high level of surface functionalization which was also evident from subsequent further derivatization techniques to convert the hydroxyl groups to other functionalities (trimethylsilyl (see Figures 2-12 and 2-13), nitro and amine groups) and to couple chromophores. Hydroxylated polystyrene microspheres were found to be susceptible to intermolecular association (aggregation) which both impeded realization of monolayer chromophore coupling and the realization of desired morphological resonances. Such aggregation could be viewed by SEM (Figures 2-10 and 2-11). We also achieved hydroxylation of microspheres employing a free radical mechanisms shown in Figures 2-6 to 2-8. As is seen from Figures 2-14 and 2-15, comparable results were obtained. Thus, while this approach yielded, with great syntheric care, chromophore microspheres characterized by essentially monolayer chromophore coverage, it was abandoned due to aggregation problems.
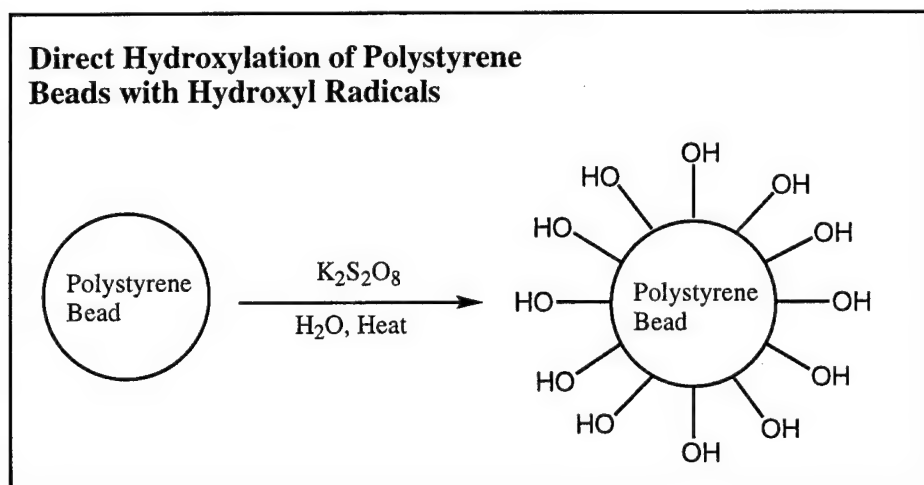
Figure 2-6. Direct hydroxylation of preformed polystyrene microspheres via hydroxy-radical mediated surface modification.

Hydorxylation of Aromatics

$$Ar\text{-}H \xrightarrow[H_2O_2]{\text{Strong Acid}} Ar\text{-}OH$$

$$H_2O_2 + HX \longrightarrow H_3O_2^+X^-$$
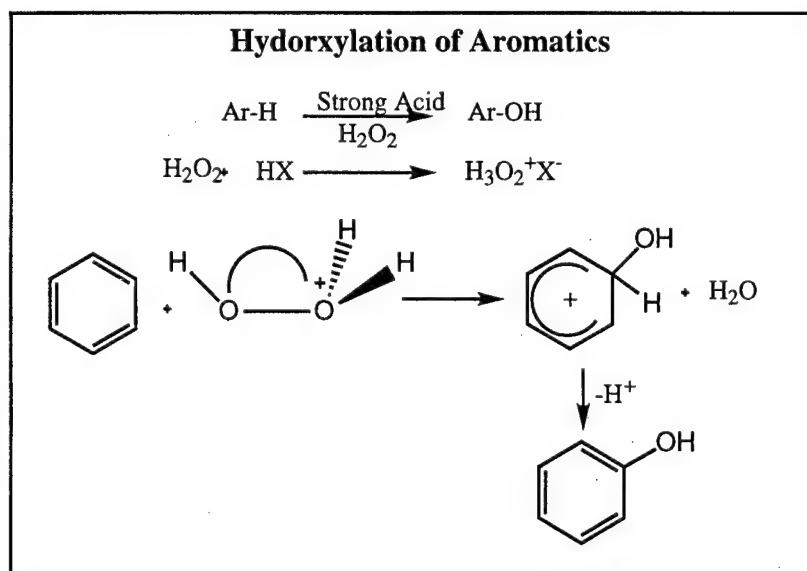
Figure 2-7. Direct hydroxylation from hydroxy radicals generated via hydrogen peroxide and a strong acid.
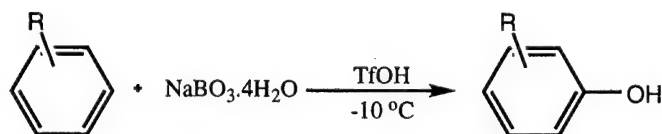
Table 1. Hydroxylation of aromatic compounds with sodium perborate/trifluoromethanesulfonic acid

substrate	rxn. temp. (^{o}C)	mono- hydroxy product, yield (%)	isomer distribution		
			ortho	meta	para
benzene	rt	62			
toluene	-10	66	65	9	26
ethylbenzene	-10	68	65	11	24
o-xylene	-10	57	48(2,3)	14(2,6)	38
p-xylene	-10	70	70(2,5)	30(2,4)	
mesitylene	-10	73			
chlorobenzene	-10	71	32	9	59
anpththalene	-30	70	67(a)	33(β)	

carried out in CHCl with substrate/reagent ratio of 2:1

Figure 2-8. A third method used for the direct hydroxylation of polystyrene microspheres, using hydroxy radicals.

16

Infrared Spectra of Hydroxylated Microsphere (top reaction in chlorobenzene, bottom, reaction in methylene chloride)
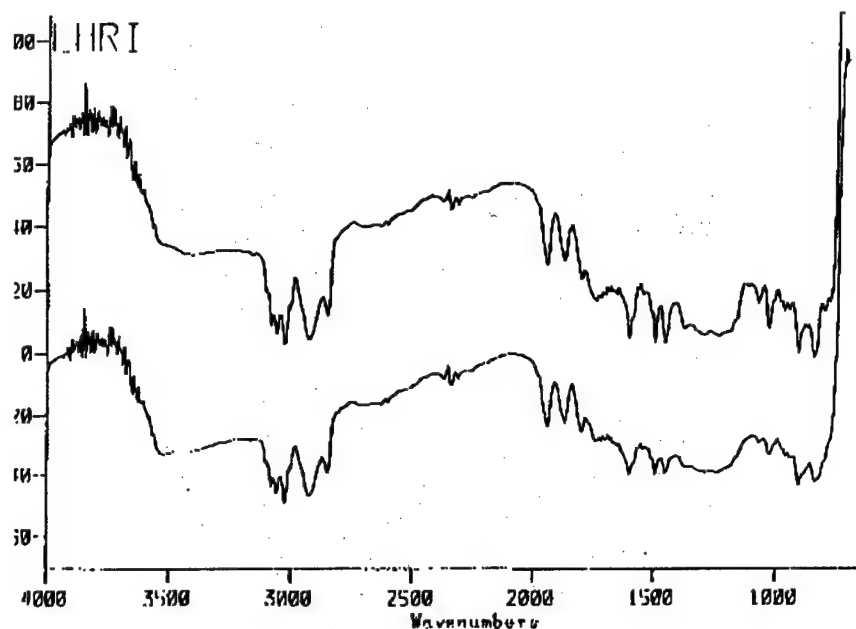
Figure 2-9. Infrared spectrum of hydroxylated microspheres (top: reaction in chlorobenzene; bottom: reaction in methylene chloride).
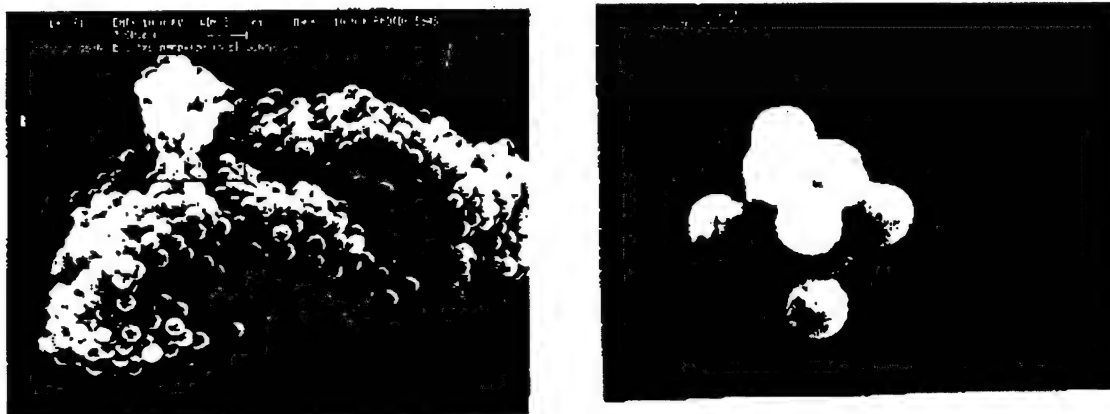
Figure 2-10. Scanning electron micrographs of precursor microspheres and hydroxylated microspheres using hydroxyl radicals. *This sample was prepared according to figure 9, in chlorobenzene.*

Figure 2-11. Scanning electron micrographs of precursor microspheres and hydroxylated microspheres using hydroxyl radicals. *This sample was prepared according to Figure 9, in methylene chloride.*
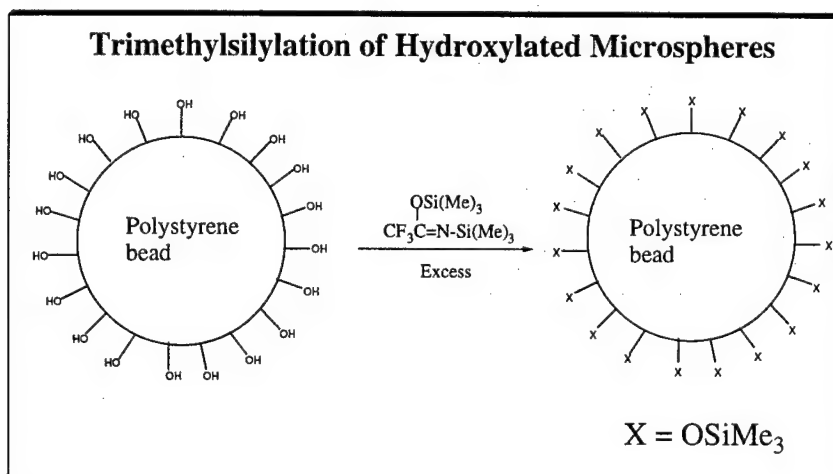
Figure 2-12. Surface modification of hydroxy-functionalized polystyrene beads. *This example shows the trimethylsilylation of the surface.*

18

Infrared Spectra of Hydroxylated Microsphere (top) and after Trmethylsilylation (bottom)
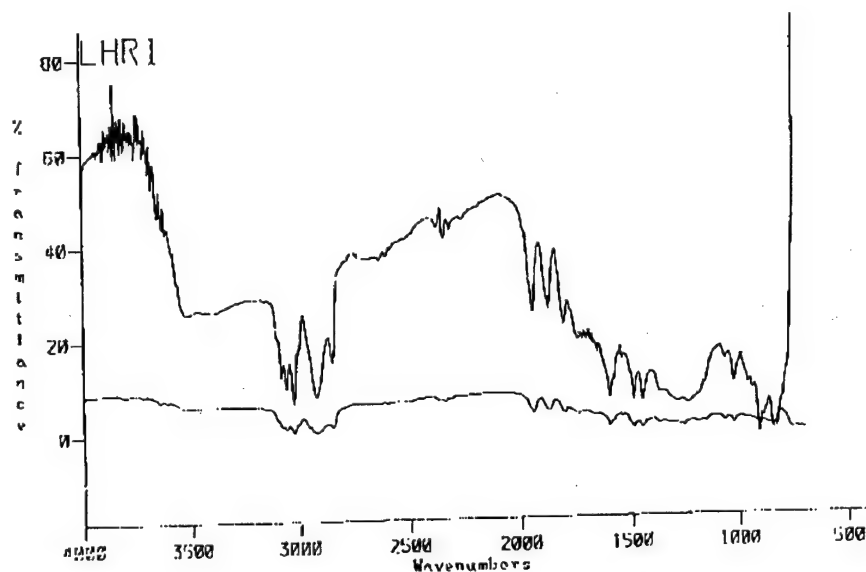
Figure 2-13. Infrared spectra of hydroxylated microsphere before (top) and after (bottom) trimethylsilylation.

Infrared Specta of Hydroxylated Microsphere using Hydroxyl radicals
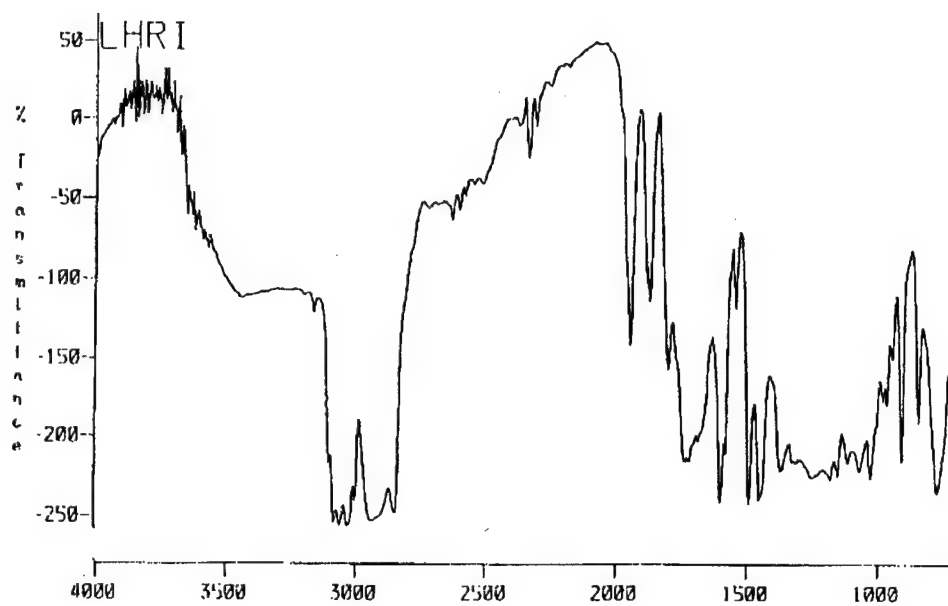
Figure 2-14. Infrared spectra of polystyrene microspheres functionalized via hydroxyl radicals, to give a hydroxylated surface.
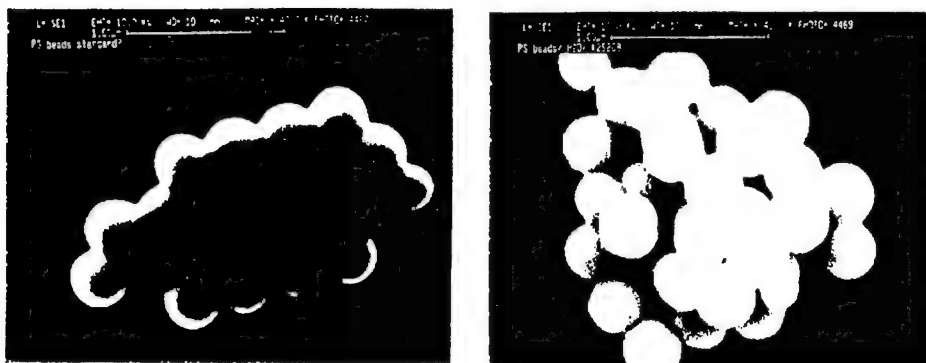
Figure 2-15. Scanning electron micrographs of polystyrene micro-spheres functionalized via hydroxyl radicals, to give a hydroxylated surface.

Aminated polystyrene microspheres were prepared by two approaches. Polystyrene microspheres undergo smooth surface nitration which upon boron hydride reduction leads to aminated polystyrene microspheres (Figure 2-16).
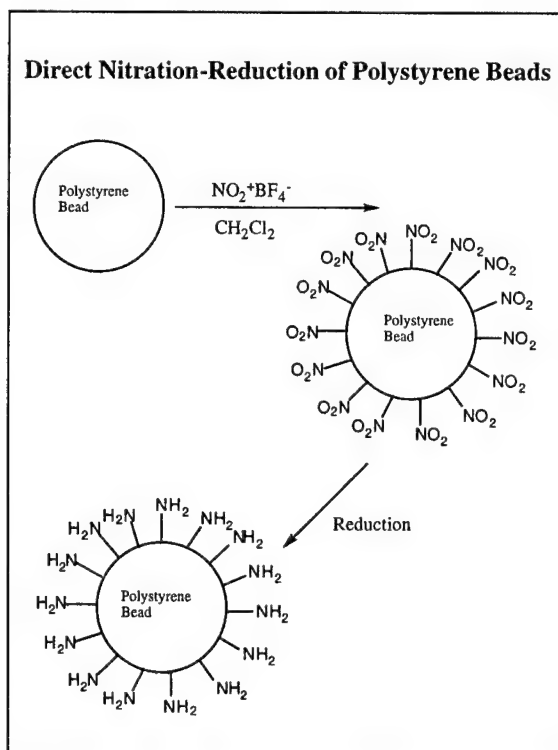
Figure 2-16. Surface amination of polystyrene microspheres via two-step surface nitration-reduction.

Direct amination was achieved by reaction of preformed microspheres with an organic azide in strong acid (Figure 2-17).

Aminated polystyrene microspheres were found to be much more aminable to subsequent chemical modification including the coupling of chromophores (Figure 2-18). With aminated polystyrene and functionalized polystyrenes synthesized from aminated polystyrenes, we were able to obtain monolayer chromophore coating of high crosslink density microspheres.

The synthesis of surface functionalized polystyrene microspheres was accompanied by the synthesis of asymmetrically functionalized azobenzene chromophores. Chromophores were of a donor-acceptor nature with an amine donor group in the 4 position and a sulfonyl acceptor group in the 4-foot position of azobenzene. This structure was utilized because we had previously demonstrated that this gives rise to a high fluorescence yield unlike underivatized azobenzenes. The asymmetric functionalization also permitted the controlled coupling of a single chromophore layer to the surface of polystyrene microspheres and the stepwise build up of chromophore layers one layer at a time. Such functionalization was also useful for increasing the solubility of azobenzene in polar solvents and mixed solvent systems.

Direct Amination of Polystyrene Beads

Polystyrene Bead → $(CH_3)_3SiN_3$ / CF_3SO_3H, CH_2Cl_2 → Polystyrene Bead with H_2N / NH_2 groups
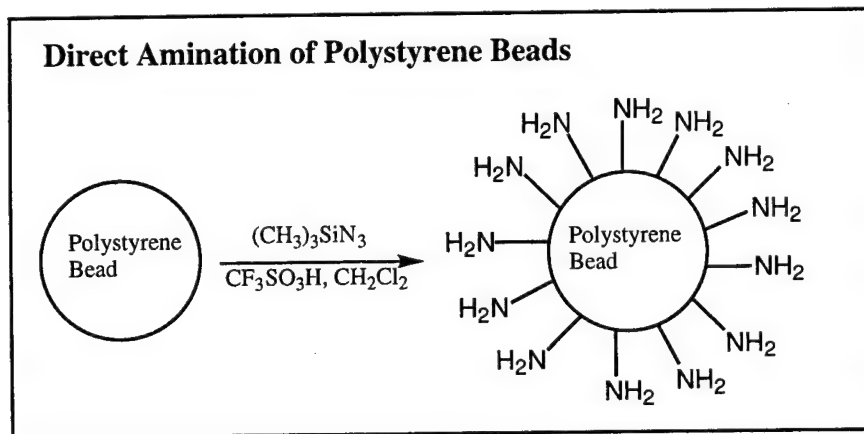
Figure 2-17. Direct one-step surface amination of polystyrene microspheres using trimethylsilylazide and a strong acid.

Coupling at Bead Surface with Chromophores

Polystyrene Bead

chromophore
X = Cl, Br, CNO, etc.

Chromophores can be attached- monolayer thick
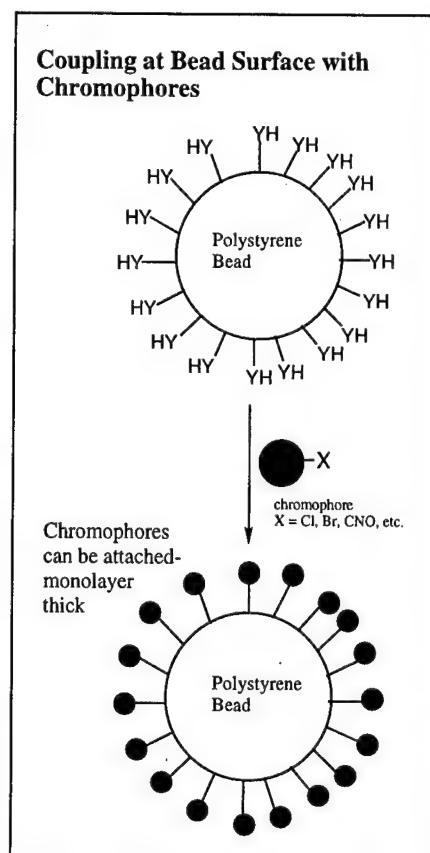
Polystyrene Bead

Figure 2-18. Monolayer incorporation of chromophores onto microsphere surfaces. *This method works best for amine surface-fuctionalized polystyrene microspheres.*

Our continuing studies of azobenzene materials revealed a fatal shortcoming of these systems—a problem that we have observed to effect most organic photochromonic materials—namely, unacceptably slow kinetics for writing and erasing information (i.e., for photoconversion of the chromophore from one conformation to the other). To address this problem and also to attempt to improve signal to noise by identifying chromophores which are highly fluorescence in one conformation but not the other, we undertook the synthesis of new classes of photochromonic materials.

At this point, some general comments on chromophore design are warranted. Structure/function relationships for fluorescence efficiency and conversion efficiency for organic materials are complex and have never been quantified by anyone with the exception of definition of the heavy atom effect on fluorescence efficiency (not applicable here) and the observation of a general (qualitative) relationship between conversion efficiency and steric hindrance involving nearby groups. This is the problem which plagued us. One simply must adopt the "Edisonian approach," which involves the preparation and screening of a great many compounds to have any hope of improvement.

Also, regarding switching times, we observed no improvements over existing materials, but the new materials were complicated by photodecomposition which prevent a meaningful assessment of either conversion efficiency or fluorescence efficiency.

Before we review our efforts on chromophore development, it is appropriate to summarize our observations concerning the development of functionalized microsphere surfaces. It was our clear experience that the most successful route to microspheres with both a high degree of surface functionalization and a high degree of crosslinking is to effect functionalization of preformed beads. This approach permits the preparing of functionalized beads sufficiently robust as to permit a variety of chemical reactions to be effected. Such beads may have utility in photoelectrochemical cells and as supports for catalysts and for sequential synthesis methods.

2.2 PHOTOCHROMOPHORE STUDY

2.2.1 Synthesis of Thioindigo Photochromophore

The synthesis of thioindigo **4** was carried out in three steps, according to Figure 2-19. The starting material thiophenyl-acetic acid **1** was purchased from Aldrich and was used without purification. The synthesis started with the conversion of **1** into the acyl halide **2**. Compound **2** was transformed into **3** by the Friedel-Craft's ring-closing reaction. The final product, thioindigo **4**, was synthesized by the self condensation of **3** in refluxing thionyl chloride. The reaction scheme, shown below, initially seemed straightforward. Whereas, due to the extremely sensitive conditions of reactions, each step was carried out for several times in order to establish the optimum synthesis conditions.
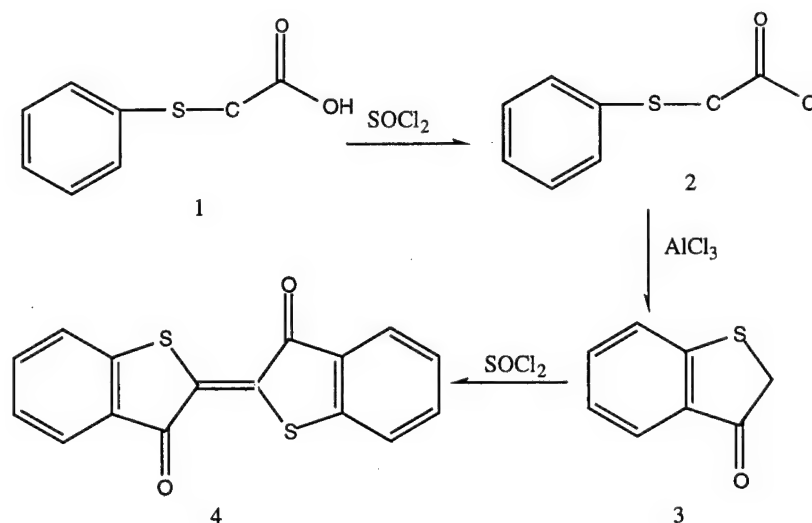
Figure 2-19. Synthetic scheme for the preparation of the thioindigo photochromophore.

The detailed, optimized procedure is as follows. Thiophenyl-acetic acid (18.3 g, 0.1 mol) and 30 ml of $SOCl_2$ were mixed in a 100 ml RB flask, and were refluexed at 80°C until no further hydrogen chloride evolved. Excess thionyl chloride was removed via vacuum distillation, and the crude product was used without further purification. The material was redissolved in o-dichlorobenzene (80 mL) and transferred to a 125 mL addition funnel. The solution was added to a flask filled with 20 grams of anhydrous $AlCl_3$ and 300 mL of o-dichlorobenzene. An icebath was used to maintain the temperature around 0°C. Upon completion of the addition, the temperature was allowed to gradually rise to 40°C and was maintained at that temperature for 1 hour. The mixture was poured slowly into a 1.0 L beaker filled with iced NaOH solution. The organic phase was collected and washed with $NaHCO_3$ (5%). After removal of o-dichlorobenzene, a dark red viscous oily material was obtained. The crude product was purified via recrystallization in hexane, giving red monoclinic crystal (11 grams, yield 73%). One gram of the product was placed in a 100 mL RB flask and refluxed with 5 mL of thionyl chloride for 2 hours. Dark red powder product was obtained upon removal of excess thionyl chloride. Enantiomerically pure E-thioindigo was confirmed by FT-NMR.

The synthesis of compound 4 was extremely difficult due to solubility problems. The ring-coupling reaction was found to be very sensitive to moisture and temperature. If the reaction conditions were not very well controlled, many side products were produced which makes the isolation of the product from the reaction mixture rather difficult. Compound 3, the precursor of 4, was synthesized via Friedel-Craft's acylation, which commonly resulted in low yields. Strictly anhydrous conditions were found to be extremely important, as the presence of the moisture invariably resulted low yields and side products. It took many trials to find the optimal conditions for the purification of compound 3. It was also necessary to repeat the purification several times in order to obtain highly pure product, which was essential for the final coupling step to yield the target thioindigo photochromophore.

2.2.2 Material Characterization

2.2.2.1 Experimental Setup. The experimental setup was basically the same to what have been reported previously. In order to improve the room temperature spectral-hole burning process, a laser intensity stabilizer was added to the system (illustrated in Figure 2-20) to reduce the intensity noise from the excitation laser. Over the 30-nm scanning range the stabilizer basically clamps the output intensity close to a constant level (as shown in Figure 2-21). In addition, the stabilizer also reduces the noise level by roughly a factor of 2.
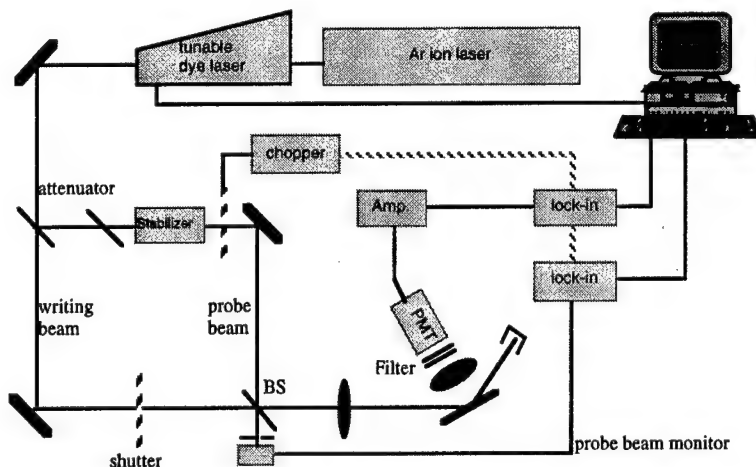
Figure 2-20. Basic experimental setup for evaluating room-temperature DLMS-based memory operations. *An external intensity stabilizer was added to the system to clamp the excitation intensity.*
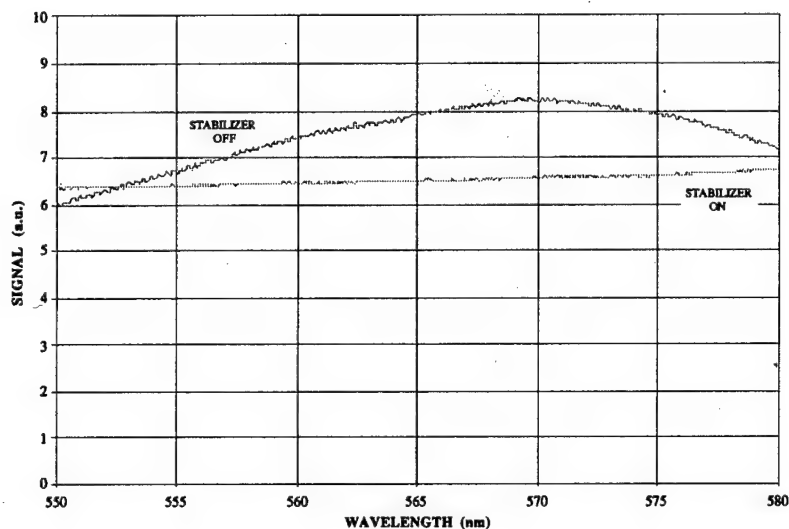
Figure 2-21. The intensity stabilizer clamps the excitation intensity to be roughly constant. *In addition, the stabilizer also improve the laser fluctuation noise.*

2.2.2.2 Fluorescence Measurement. As a photoreversible chromophore the E-state thioindigo will be photo-converted into Z-state thioindigo by laser source. The transformation should be reflected by a shift in absorption peak (from 550 nm to around 480 nm). Since the fluorescence state of Z-state is virtually zero, fluorescence measurement was also used to estimate the photoconversion efficiency. A thin-cell (1-mm depth) was acquired to evaluate the photo-conversion process, thus only a small amount of solution (thioindigo in $CHCl_3$ solvent;

25

concentration: unknown) was used for testing. To conduct a quick testing we simply chose excitation wavelength $\lambda \approx 550$ nm and intensity ≈ 400 mW/cm^2. Preliminary characterization indicated that the fluorescence efficiency was strong and signal could be easily detected. The measured fluorescence spectrum, measured by Spectrascan Model PR–713/PC from Photo Research, is shown in Figure 2-22. This information is critical for the choice of optical filters to be used to block scattered light, which is the major source of background signal, from the fluorescence signal. In general, it is necessary to have enough spectral separation between the excitation source and the maximum of fluorescence emission. High extinction color filters with cutoff wavelength longer than 600 nm are good choices for this material.

After a long exposure time ($\approx$ 4 hours) we did visually observe color change in solution. The absorption spectrum failed to provide a clear, distinctive shift (550 nm —> 480 nm). The "apparent" conversion efficiency and conversion speed were far too low to be practically useful. We also tested the photo-conversion process with thioindigo dispersed in polymer (both $\approx 1\%$ and $\approx 4\%$ concentration). Similar to the sample in CHCl$_3$ solvent, the fluorescence decay rate was fairly slow (as shown in Figure 2-23). No significant optical change was even observed.

THIOINDIGO IN CHCl$_3$
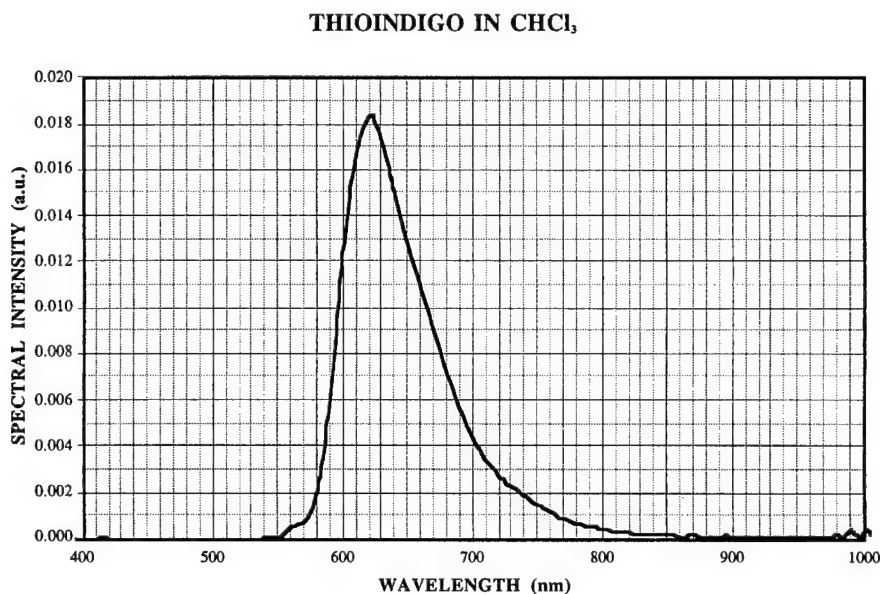
Figure 2-22. Typical fluorescence spectrum of thioindigo in CHCl$_3$ solvent.
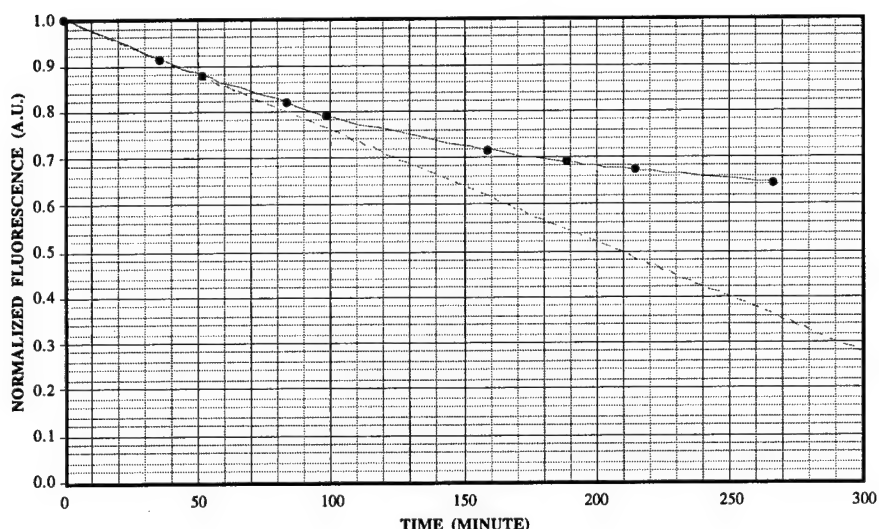
Figure 2-23. Fluorescence decay measurement for sample with thioindigo ($\approx$ 4 %) dispersed in polymer.

2.2.2.2 Preliminary Photochromic Evaluation. The optical spectra of *E*-thioindigo in chloroform, poly(methylmethacrylate) (PMMA), and Epoxylite are shown in Figures 2-24, 2-25, and 2-26, respectively. Also shown are the bleaching characteristics of thioindigo, associated with the photoisomerization of thioindigo from the *E*-isomer to the *Z*-isomer, in PMMA and Epoxylite. These are shown in Figure 2-27 to Figure 2-32, for thioindigo in PMMA. Various exposure times at 532 nm (frequency-doubled Nd:YAG) in PMMA result in the disappearance of the E-isomer (peak at 540-548 nm), with a peak appearing that corresponds to the Z-isomer (peak at 474 to 478 nm). Upon irradiation at 532 nm, the exposed regions were observed by the eye to turn from pink to colorless. Similar results were obtained from the Epoxylite/thioindigo materials. One puzzling observation was the appearance of other peaks upon irradiation. It is unclear at this point as to the nature of these extraneous absorptions, as their presence and/or intensities were invariant with respect to exposure intensities or durations.
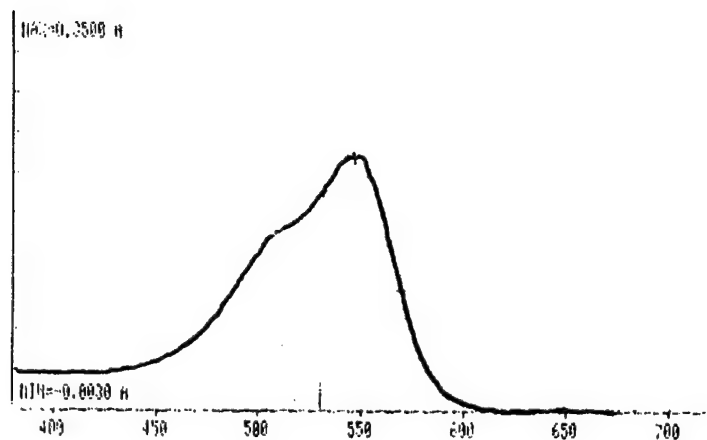
Figure 2-24. Absorption spectrum of Thioindigo in CHCl$_3$
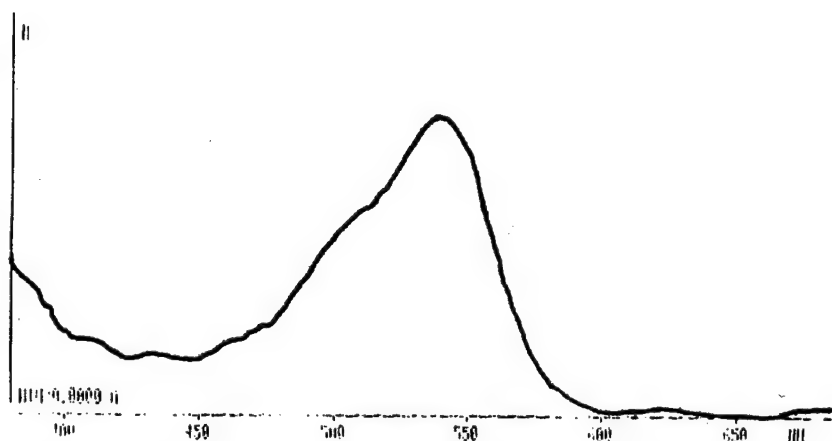
Figure 2-25. Absorption spectrum of Thioindigo in PMMA
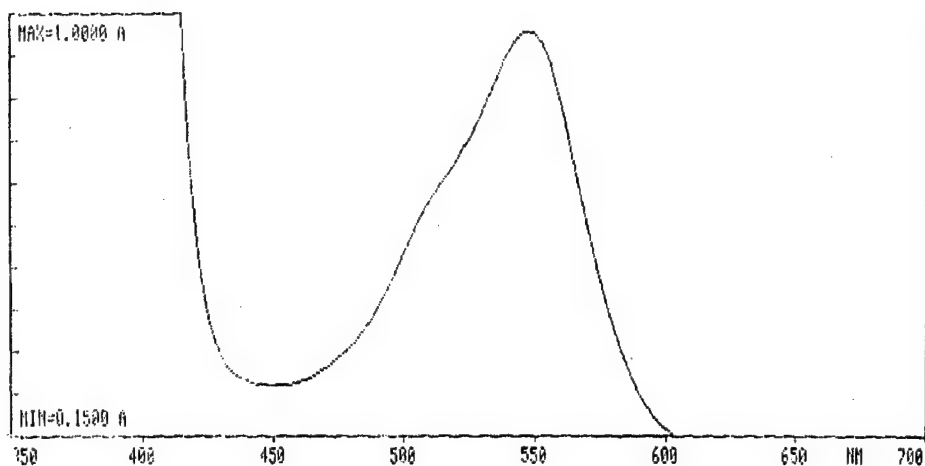
(To be changed)
Figure 2-26. Absorption spectrum of Thioindigo in Epoxylite.

28

To examine the reversibility of photoisomerization, the bleached regions were irradiated at 515 nm (Ar-ion output), which corresponds to the absorption region of the Z-isomer of thioindigo. For both the PMMA and Epoxylite/thioindigo composites, the disappearance of the Z-isomer peak was observed, along with the reemergence of the E-isomer peak. This is shown in Figures 2-33 and 2-34 for PMMA and Epoxylite samples, respectively. However, this "erase" cycle was found to be non-quantitative. Preliminary indications are that this may be due to photo-decomposition and/or photochromophore immobility. The latter case may arise due to the fact that the extremely rigid lattice (a heavily crosslinked lattice), which was necessary to prevent sublimation of the thioindigo, most likely hinders the isomerization mode, in that the di-radical intermediate generated as a transient species in the photoisomerization mechanism preferentially recombines to reform the original isomer, since it is difficult to configurationally isomerize before radical recombination. This process is shown in Figure 2-35.
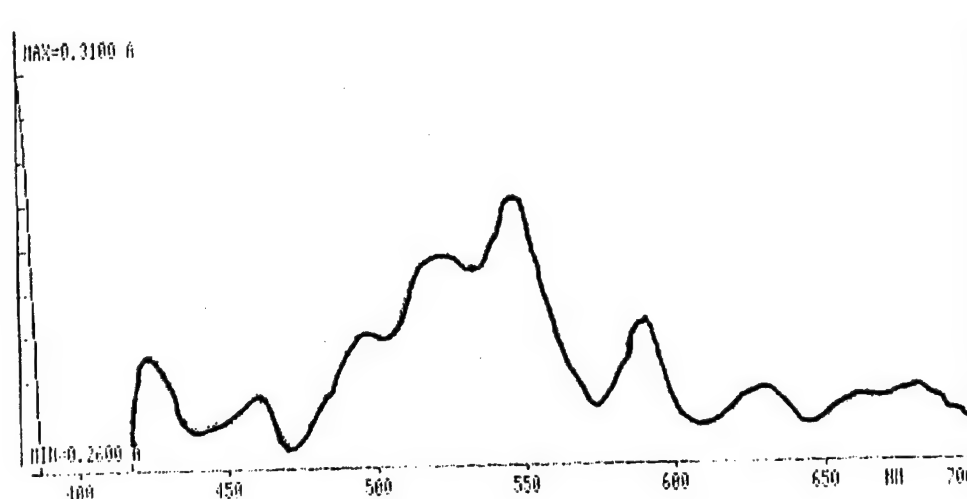
Figure 2-27. Absorption spectrum of thioindigo/PMMA composite, after irradiation at 532 nm for 30 seconds.
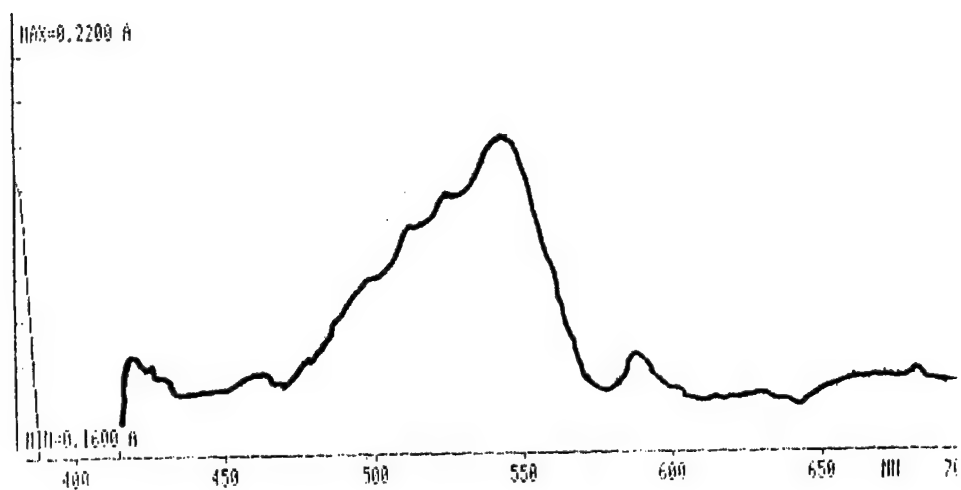
Figure 2-28. Absorption spectrum of thioindigo/PMMA composite, after irradiation at 532 nm for 2 minutes.
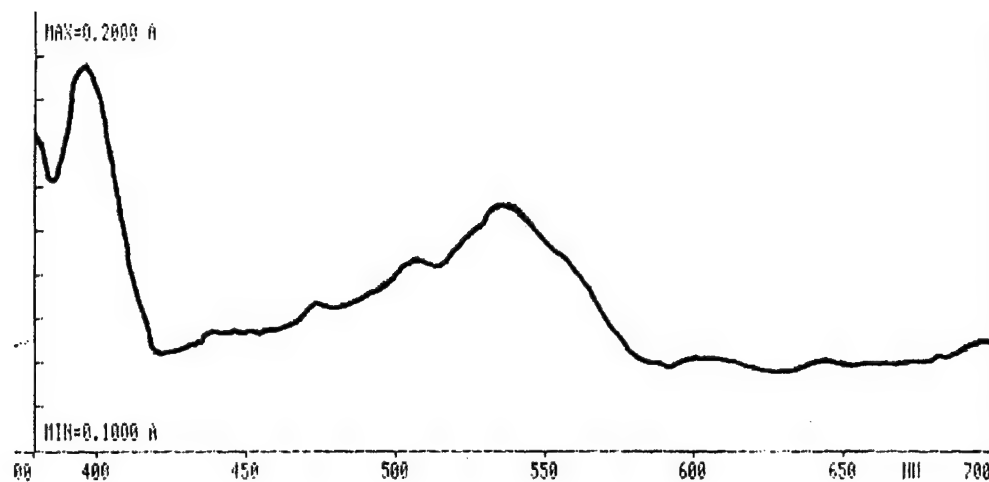
Figure 2-29. Absorption spectrum of thioindigo/PMMA composite, after irradiation at 532 nm for 6 minutes.
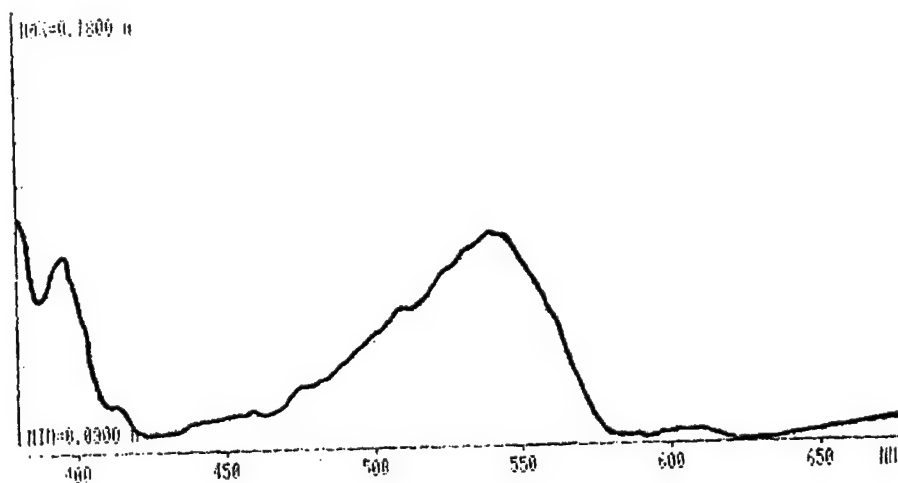
Figure 2-30. Absorption spectrum of thioindigo/PMMA composite after irradiation at 532 nm for 10 minutes.
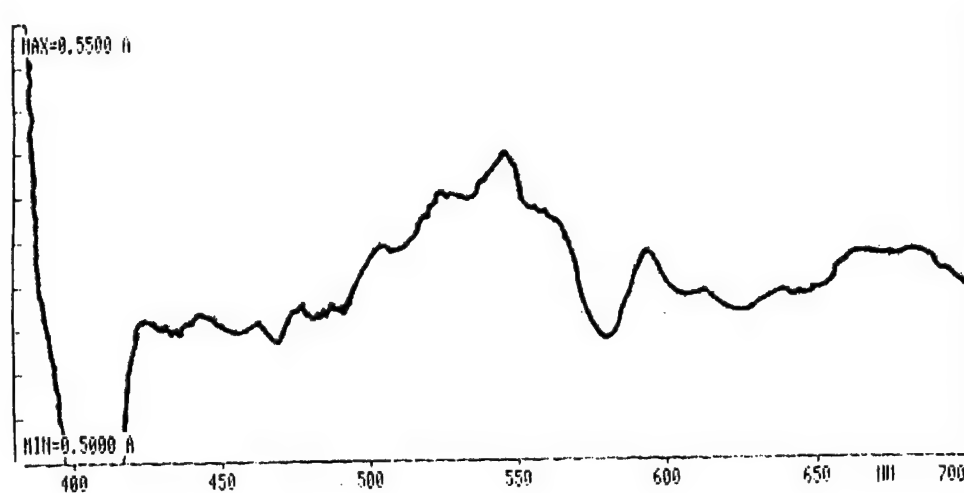
Figure 2-31. Detailed absorption spectrum in the bleached region of Figure 2-30.
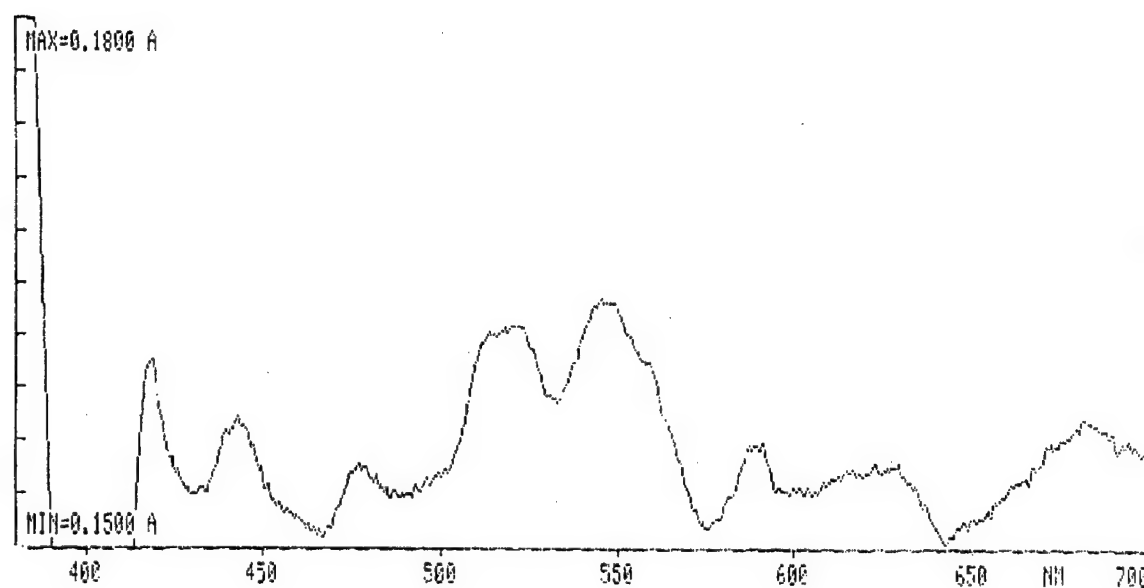
Figure 2-32. Absorption spectrum of thioindigo/PMMA composite, after Irradiation at 532 nm for 30 minutes.
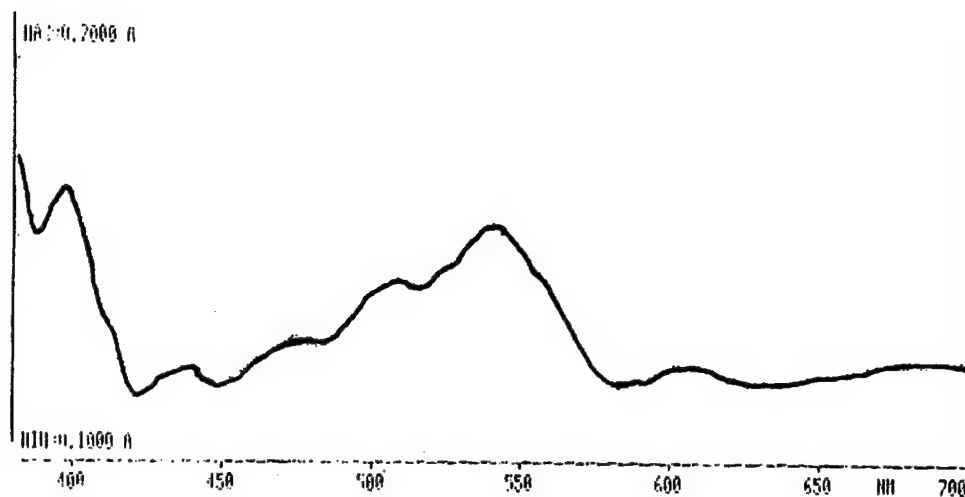
Figure 2-33. Irradiation at 515 nm of the bleached region of a thioindigo/PMMA composite, showing the reemergence of the E-isomer peak.
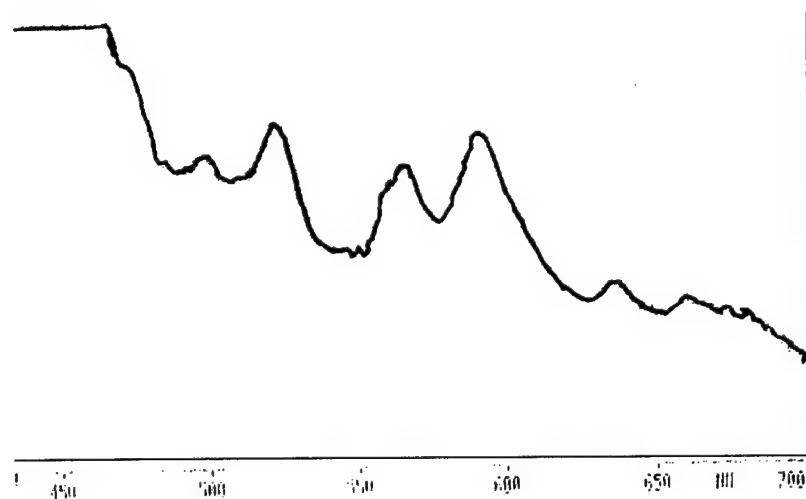
Figure 2-34. Irradiation at 515 nm of the bleached region of a thioindigo/Epoxylite composite, showing the reemergence of the *E*-isomer peak.
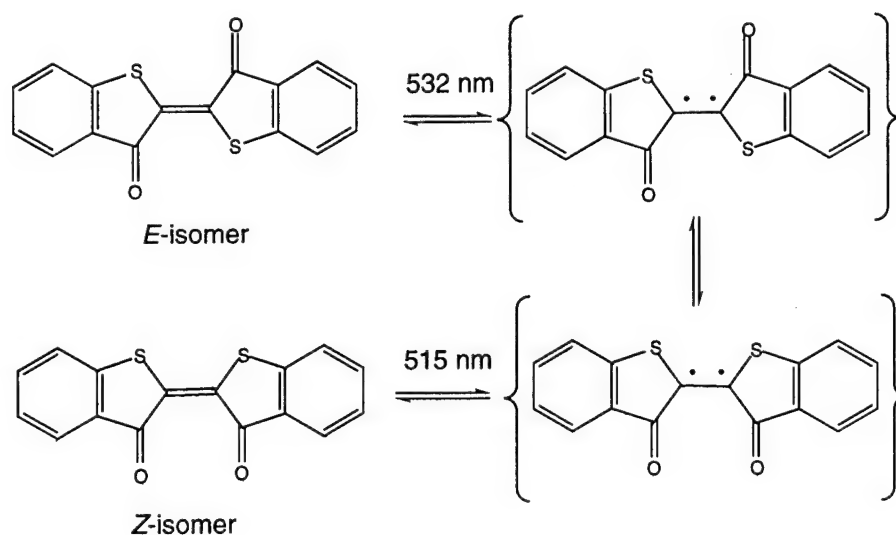
E-isomer

Z-isomer

Figure 2-35. Photoisomerization mechanism for thioindigo.

It is probably safe to say that rigid lattices reduce conversion efficiency and may impede somewhat (not as much as we had hoped) photodecomposition but accurate measurements were impossible because photodecomposition could not be eliminated. Since we could not obtain a system without photodecomposition, we could not identify a material to optimize for device demonstration thus it was meaningless to focus on the shifting of the chromophores' absorption maxima by synthesizing chromophores with enlarged pi-electron clouds.

33

The take-home lesson is that achieving organic photochromism is a major problem for the organic optical memory development. The problem of photo-instability is serious and it probably is not possible to increase switching speeds unless materials with a radically new mechanism are identified. I doubt if materials undergoing isomerization, ring opening reactions, or tautomerism will ever be found that switch on sub millisecond time scales. In all of the materials which we studied (with the exception of the azobenzenes) some photodecomposition was observed before switching was observed. We tried the full range of conditions from solutions to epoxies to try to identify a materials where switching could be achieved without photodecomposition.

Section 3
THEORETICAL STUDY

Sharp MDR's associated with microspheres provide the fundamental room temperature wavelength multiplexing tool. When the size parameter of a particular dye-labeled microsphere matches natural resonant conditions, the internal optical field near the microsphere surface grows relatively intense.[1] On the other hand, the field inside the microsphere approaches being a constant when the resonance conditions are not matched. The enhanced photon-absorption in the microspheres matching the resonance conditions will preferentially promote photo-isomerization. For example, an azobenzene chromophore is more likely to undergo trans-to-cis isomerization if it is labeled on a microsphere that matches a morphological resonance at the wavelength in question. Such enhancement reaction will not be observed for the dye attached onto microspheres that do not match the MDR's.

Increasing the Q-factors of the morphology-dependent resonances (MDR's) will allow highly defined frequency slots to be "burned" with a low intensity tunable laser. Thus, to enhance the data storage capacity it is critical for the DLMS features with high Q-factor. To facilitate more understanding on how the characteristics of dye-labeled microspheres may affect MDR's, we conducted a theoretical study on MDR's. First, for general MDR analysis we simplified the modeling and only considered DLMS homogeneous microspheres. This simple model allows us quickly estimate the Q-factor of MDR's, and thus the multiplexing factor of the frequency channels may be supported in the DLMS. Next, we extended the general modeling to layer-structured microspheres, that is a thin layer of bi-stable dye coupled to homogeneous microspheres.

3.1 SIMPLIFIED MODEL–HOMOGENEOUS MICROSPHERES

The homogeneous microspheres is the simplest and most general form of scatter has been considered in the literature. Following Mie scattering theory, the MDR's of a homogeneous microsphere may be characterized once its refractive index ($m = \mathbf{Re}(m) - i\,\mathbf{Im}(m) = m_R - i\,m_i$) and the size parameter ($x = \frac{2\pi a}{\lambda}$), here a is the radius of the microsphere and λ is the optical wavelength) are known. At resonance, standing waves are formed by counterpropagating surface waves traveling along the boundary of the microsphere and its surrounding media. Note that the refractive index m is normalized with respect to that of its surrounding. The MDR's are generally characterized by the mode number (n) and the order number (l). The order number n represents the number of relative maxima in the standing wave along the half circle circumference. The order number l indicates the number of relative maxima in the radial distribution in the internal optical field. Both transverse electric (TE-mode) and transverse magnetic (TM-mode) resonances exist,

but occurring in different resonance size parameters. Please refer References (2) and (3) for detailed calculation information about Mie scattering.

MDR occurs when the size parameter is resonant with the natural modes of oscillation characteristics of the microsphere. The Q-factor of the MDR may be defined to be $x_{MDR}/\delta x_{MDR}$, here x_{MDR} and δx_{MDR} are the location and the corresponding resonance linewidth expressed in size parameter. In a perfect microsphere the effective Q-factor may approach 10^6, or even larger. This is the fundamental basis for choosing MDR's as the precision wavelength multiplexing tool.

3.1.1 Effect of Refractive Index

The characteristics of MDR's are found to be sensitive to the refractive index of the microspheres. Figure 3-1 clearly illustrates that, within the same size parameter range, sharper MDR's may be observed for the microspheres with higher refractive index. The total scattering cross-section, Q_{sca}, is given as a measure of the scattering efficiency. Note that the separation between each MDR is also highly reduced when higher order MDR's are excited. That will impose some limitations on the effective data storage density the system may achieve. The simulation also indicates that if the high optical induced by the MDR could cause some change in $\mathbf{Re}[m]$, the locations of MDR's will experience shifts in size parameters. That simply implies that we should observe a shift in the resonance wavelength.

The impacts of the refractive index on the MDR location and its corresponding resonance linewidth may be further examined from the simulations shown in Figure 3-2. For microspheres made of low refractive index (e.g., $m = 1.59$), small size parameters can only support MDR's in low n. But, the Q-factors for $n < 20$ will be too small to support a reasonable multiplexing factor. As the refractive index m is increased, the Q factors for $n > 10$ starts to provide a basis of large

Refractive index (m) = 1.3   **Refractive index (m) = 1.5**
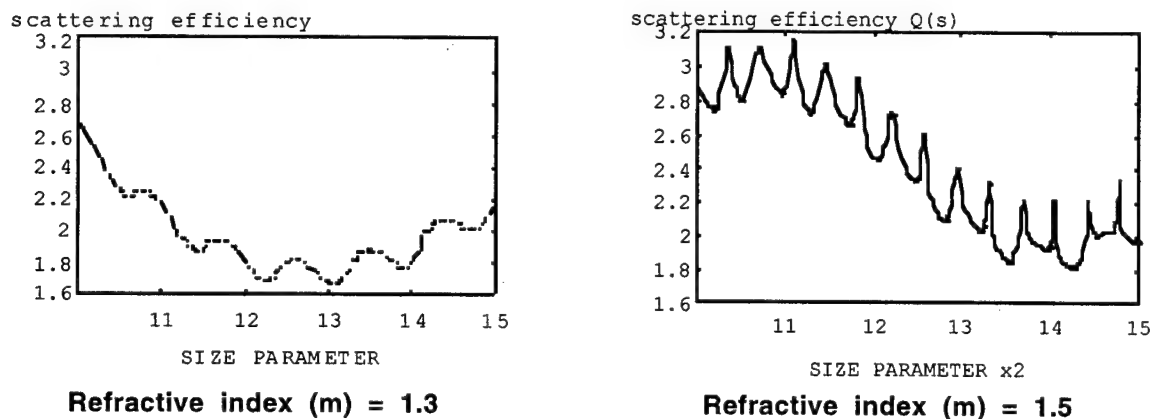
Figure 3-1. Comparison of scattering efficiencies for the microspheres in the same range of size parameter, with the exception on the difference in their refractive indices.

multiplexing factor. More important is the with higher refractive index even the MDR's in small size parameters can support fairly decent multiplexing factor. Since the size parameter is directly related to the size of microspheres, it will also determine the effective storage density of the system.

3.1.2 Effects of Material Absorption

So far we only consider lossless microspheres. Since DLMS requires chromophores with good fluorescence efficiency, this naturally implies the need of reasonably strong light absorption. Low absorption coefficient simply implies there are little excitation photons may be absorbed and then converted to fluorescence photons. The effective Q-factors of MDR's are given as

$$\frac{1}{Q_{eff}} = \frac{1}{Q_{MDR}} + \frac{1}{Q_{absf}}$$

where Q_{MDR} is the Q-factor of the lossless MDR's and Q_{abs} is the Q-factor due to absorption loss. Q_{abs} is determined by the optical absorption loss and may be approximated to be $\frac{1}{2}\frac{\text{Re}(m)}{\text{Im}(m)}$.[4] Note that the effective Q-factor may be further degraded by an additional factor, Q_{sca}, caused by non-ideal scattering losses. Even a little absorption will broaden the resonance linewidth and cause rapid degradation in Q-factor.[5] The fluorescence emitted by microspheres is appropriately related to the power absorbed.[6] The determining factor here is to optimize Q-factor for the microspheres at resonance, while minimizing the absorption at all off-resonance microspheres.

As the size parameter matches the resonance condition, the internal field inside the sphere cavity is highly enhanced (Figure 3-3). When the size parameter is slightly tuned away from the resonance condition, the field intensity is relatively small and constant within the microsphere. This field enhancement is the basic tool for allowing selectively activate the chromophore attached on microspheres.

m	MDR Location	Q-Factor of MDR's
m = 1.59	MDR Size Parameter	Q Factor
m = 2.00	MDR Size Parameter: m = 2.00	Q Factor: m = 2.00
m = 2.50	MDR Size Parameter: m = 2.50	Q Factor: m = 2.50
m = 3.00	MDR Size Parameter: m = 3.00	Q Factor: m = 3.00
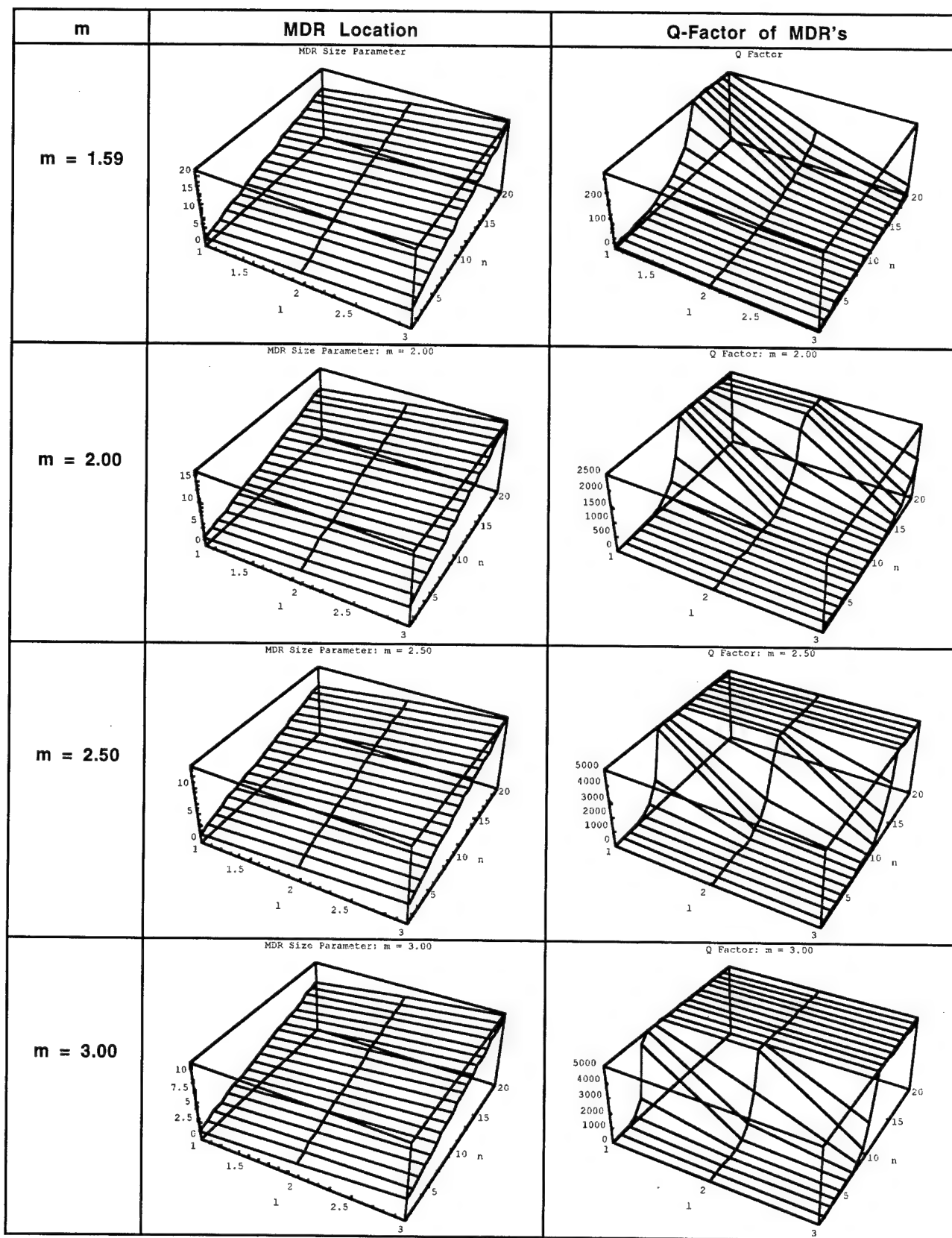
Figure 3-2. The MDR locations and the resonance widths as a function of the refractive index of microspheres.
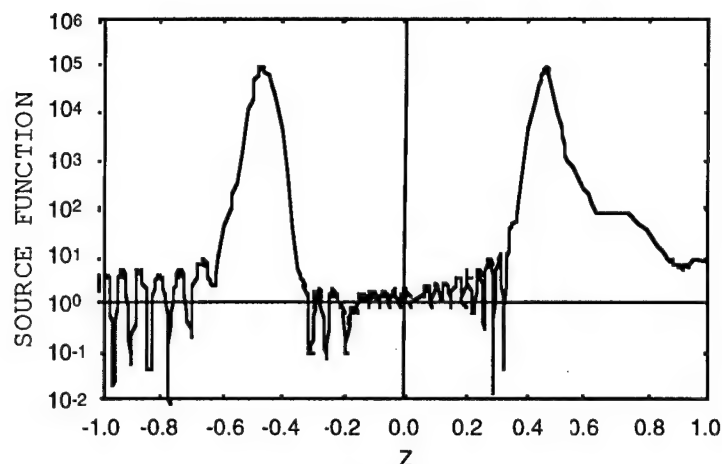
Figure 3-3. Source function (in log scale) at resonance in the $TE_{40,1}$ mode. *Here the refractive index of microsphere material = 1.47 -i 10^{-16}, the size parameter x is tuned for the resonance = 31.0588539863. The sphere-air boundaries are at z = ±0.5. (Following the cases shown in Ref. 3-7)*

In principle, we would like to have the Q-factor as large as possible. Since the Q-factor of the resonance is highly depended on the absorption coefficient of the material, the field enhancement is expected to be affected by the absorption. For α = 10/cm or more @ λ = 0.55 μm, the field enhancement is virtually disappeared (as shown in Figure 3-4). This imposes an upper limit on the light absorption the material may be used for the DLMS. It is necessary to compromise the field selectivity (high Q-factor) and the fluorescence yield. For example, although the field enhancement factor is reduced by $\approx$10 times (as shown in Figure 3-5), the given α = 1/cm @ λ = 0.55 μm may allow reasonable fluorescence efficiency. As the Q-factor is then dominated by the absorption loss, the system should have more tolerance in the imperfection of microspheres.
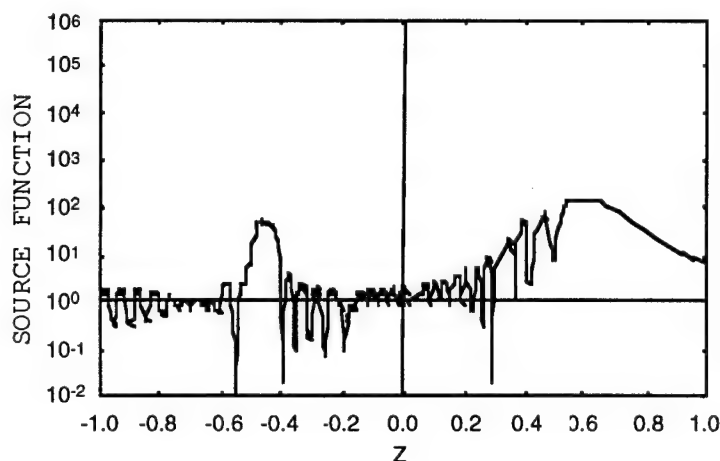
Figure 3-4. Source function (in log scale) at resonance in the $TE_{40,1}$ mode. *Here the physical conditions are kept the same as what given in Figure 3-3, with the exception that α = 10/cm @ λ = 0.55 μm.*
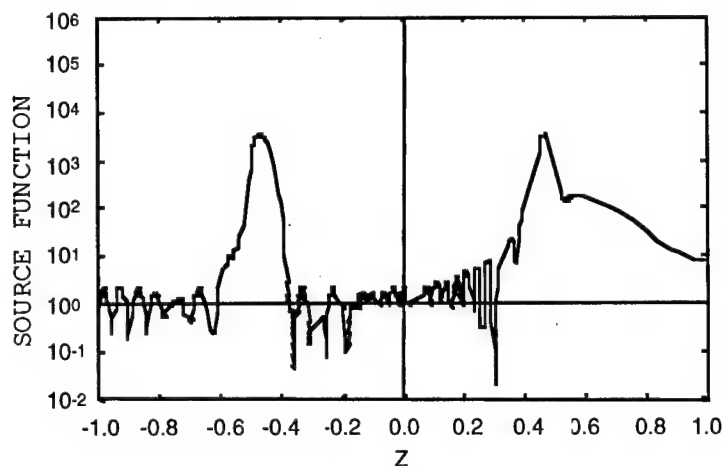
Figure 3-5. Source function (in log scale) at resonance in the $TE_{40,1}$ mode. *Here the physical conditions are kept the same as what given in Figure 3-4, with the exception that $\alpha = 1/cm$ or more @ $\lambda = 0.55$ μm.*

3.2 LAYER-STRUCTURED MICROSPHERES

Consider DLMS there exists an index discontinuity between the polymer core and the chromophore surface layer. We need to model the dye-labeled microspheres as close-to-reality layer-coated microspheres (as schematically illustrated in Figure 3-6). Light scattering in layered microspheres has been extensively studied in the past.[7-13] In this case, we followed a newly developed algorithm for computing Mie scattering characteristics.[7] The thickness and the refractive index of coating layer, relative to the core microsphere, are the key factors of interest.
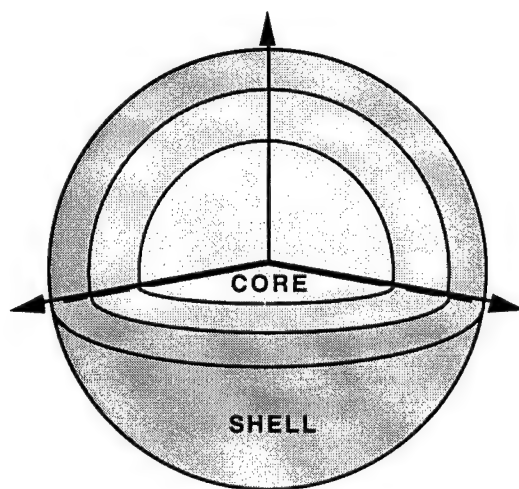
Figure 3-6. Schematic structure of a layer-coated microsphere. *The center-core will be the polymer microsphere and the dyes will be the shells attached to the core.*

To understand the effects of layer-structured microspheres, we conducted a computer simulation study. A few cases with different combinations of refractive indices for the core and coated layer were studied (Figure 3-7). As expected, the scattering efficiency experiences some degree of perturbation when a different medium replaces part of core material. When a coat layer with a lower refractive index replaces the same thickness of core medium, the MDR's suffer quickly degradation and approach the case of homogeneous microspheres composed of the same low refractive index. As the coating thickness increases, say ≈20% of the radius of the overall microsphere, MDR conditions will significantly deviate away from the core MDR conditions. And the whole composite microsphere functions like a homogeneous microsphere made of lower refractive index. This is understandable since at resonance the high-density internal optical field is distributed within this region. [3-1] Similar situation occurs when the refractive indices of both core and layer medium are reversed. Thus, if all possible, it will be beneficial to have a fairly thick bi-stable dye attached to core sphere made of low index materials. It is important to maximize the refractive index of the bi-stable dye in use.

3.2.1 Effect of Coating Absorption

We further consider the cases of absorbing coating and the results are presented in Figure 3-8. Here we simply assumed the absorptive dye is attached to transparent core medium. Thus, only the coating contributes to the excited fluorescence. As expected, with low absorption loss the characteristics of MDR's are not seriously deviated from the ideal non-absorbing cases. For bi-stable dye with low refractive index it is advantageous to make the coating thin to experience higher Q-factor. But, we could not infinitely reduce the thickness of the dye layer. After all, we need a fair amount of the dye molecules to provide fluorescence signals for effective spectral-hole detection (i.e., signal with a good S/N ratio). On the other hand, it will be better to have a thicker coating for high refractive index dyes. Both hole formation and hole detection must be achieved by optimizing the thickness of the dye-layer with the constraints of material characteristics.

	Core layer: $m = 1.3$	Core layer: $m = 1.5$
Homogeneous	Coat layer: $m = 1.3$ (homogeneous)	Coat layer: $m = 1.5$ (homogeneous)
Thin Coated Layer	Coat layer: $m = 1.5$	Coat layer: $m = 1.3$
Thick Coated Layer	Coat layer: $m = 1.5$	Coat layer: $m = 1.3$
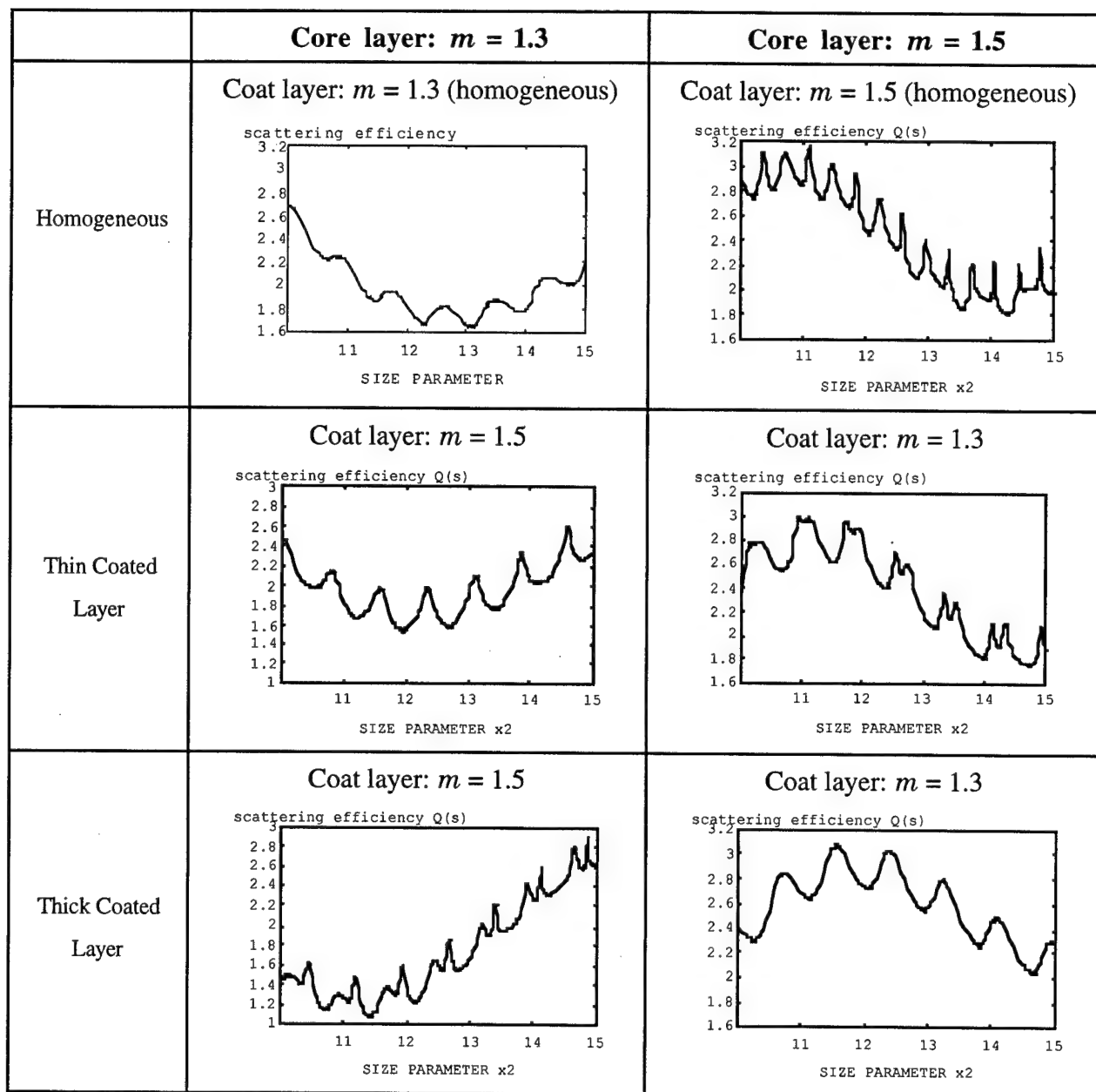
Figure 3-7. **Simulations of MDR behavior as part of core medium is replaced by a medium with different refractive index.** *The thickness of coated layer is set to be 10% (the thin coating) and 20% (the thick coating) of the radius of the overall microsphere.*

42

	Core: $m = 1.3$	**Core: $m = 1.5$**
Homogeneous	Homogeneous $m = 1.3 - i\,0.001$ scattering efficiency Q(s) 	Homogeneous $m = 1.5 - i\,0.001$ scattering efficiency Q(s)
Thin Coated Layer	Coat layer: $m = 1.5 - i\,0.001$ scattering efficiency Q(s) 	Coat layer: $m = 1.3 - i\,0.001$ scattering efficiency Q(s)
Thick Coated Layer	Coat: $m = 1.5 - i\,0.001$ scattering efficiency Q(s) 	Coat: $m = 1.3 - i\,0.001$ scattering efficiency Q(s)
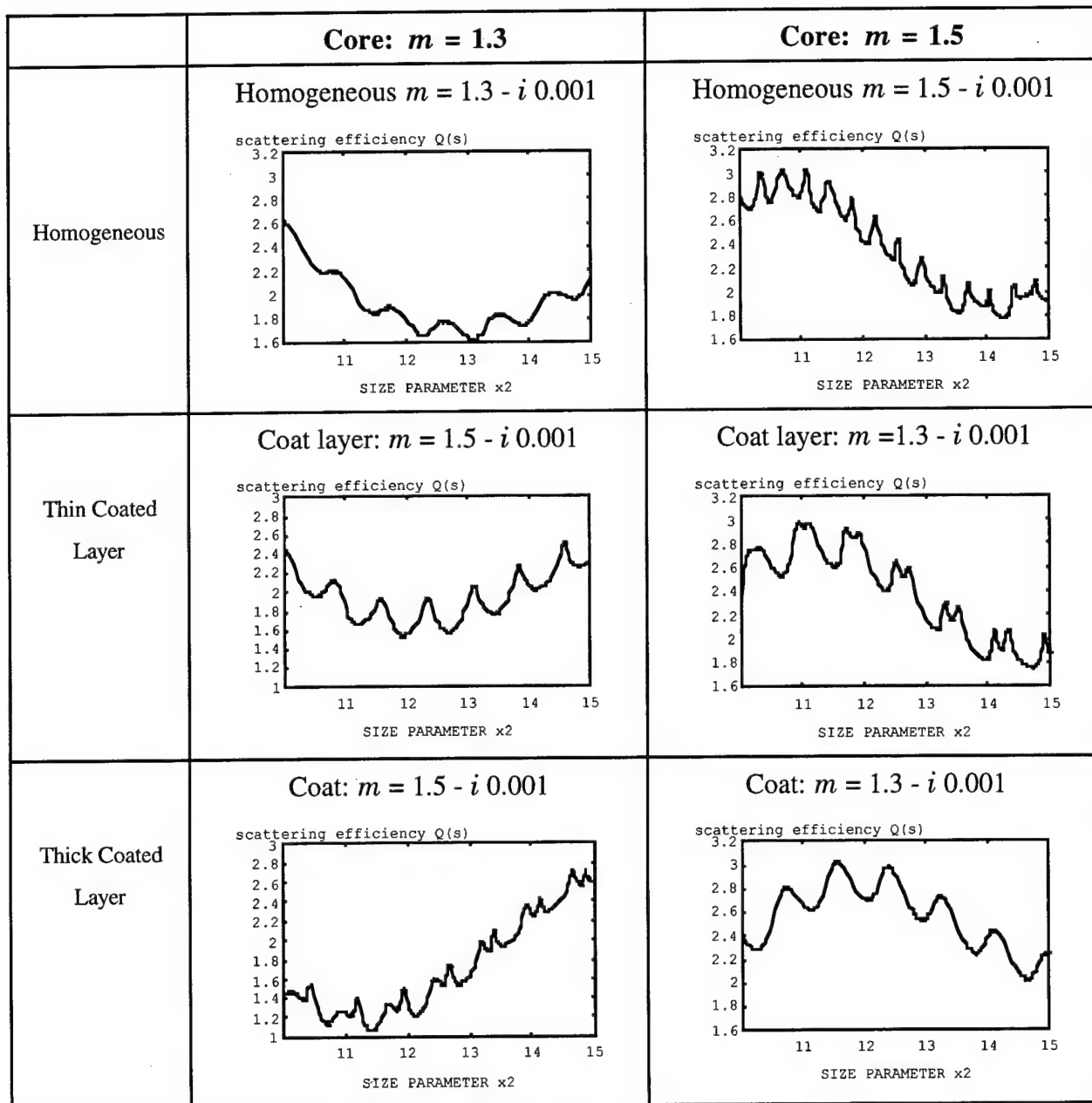
Figure 3-8. Simulations of MDR behavior as part of core medium is replaced by a medium with different refractive index. *Here the coating layer carries optical absorption loss, while the core material is assumed to be lossless. The thickness of coated layer is set to be 10% (the thin coating) and 20% (the thick coating) of the radius of the overall microsphere.*

43

3.3 MULTIPLEXING FACTOR

Wavelength multiplexing factor of the DLMS is mainly determined by how many wavelength channels may be practically squeezed into the microsphere distribution in a given pixel. For simplicity, we limit the estimation to the case that only one unique MDR mode may be supported as the excitation wavelength is scanned through its range. The restriction is given to ensure that only one MDR mode (TE-mode or TM-mode) will be excited in the operation; no multiple MDR excitation to a given microsphere will be allowed. The concept is illustrated is shown in Figure 3-9. Clearly multiple MDR excitation will simply duplicates the existing wavelength channel and provides no effective channels.
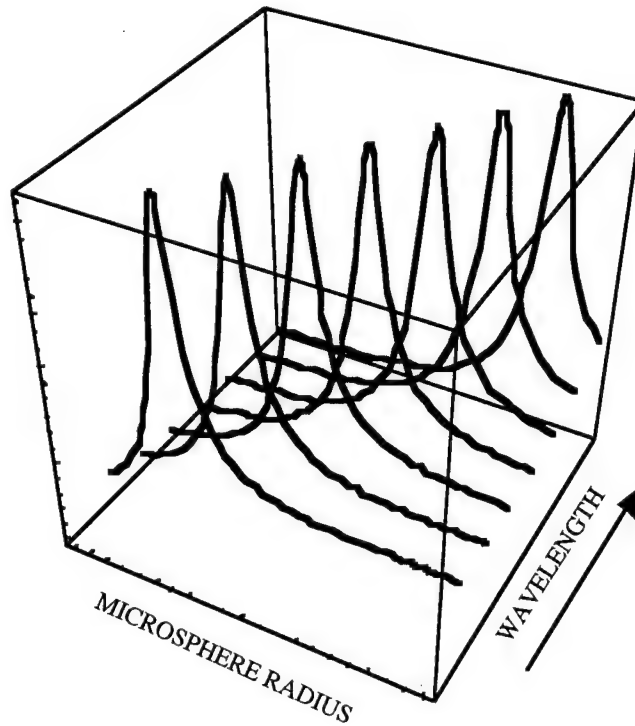
Figure 3-9. Only a unique MDR mode may be excited within the whole microsphere distribution, as the excitation wavelength is scanned through its range. *The MDR matches the wavelength to a given sub-size distribution.*

Following the above mentioned constraints, the maximum multiplexing factor may be estimated by

$$M.F. = \frac{\Delta x}{\delta x} = \frac{\Delta \lambda}{\delta \lambda}, \tag{3-1}$$

here Δx is the scanning range in the size parameter and δx is the resonance linewidth (in size parameter). Here we assume that within Δx range only one MDR mode may be excited. In general,

both Δx and δx depend on the MDR of interest. For example, both Δx and δx decreases as the size parameter of the microspheres increases (i.e., the mode number of the excited MDR increases). When the order number (l) of the MDR increases, the maximum multiplexing factor quickly degrades as δx becomes broader. It is then desired that only the low order number of MDR be excited. Unfortunately, as we reported before, the low order MDR's are sensitive to the absorption. Not only is the δx degraded by the absorption, the Q-factors of MDR's decrease too.

In the meantime we adopted the asymptotic formulas, formulated by Lam et al.,[14] for an accurate estimation of size parameters and widths of the MDR's. The information is critical for us to fairly estimate the LIMITING multiplicity factor the DLMS can even achieve. Since original asymptotic formulas only consider MDR's with large mode number, they may not accurately predict the MDR for those with small mode numbers. Table 3-1 presents the locations and the corresponding widths of TE resonances obtained numerically from Mie theory (see Figure 3-10) and the appropriated ones calculated from Lam's asymptotic formulas. The appropriate MDR locations are reasonably accurate. However, the error in resonance width can be quite large.
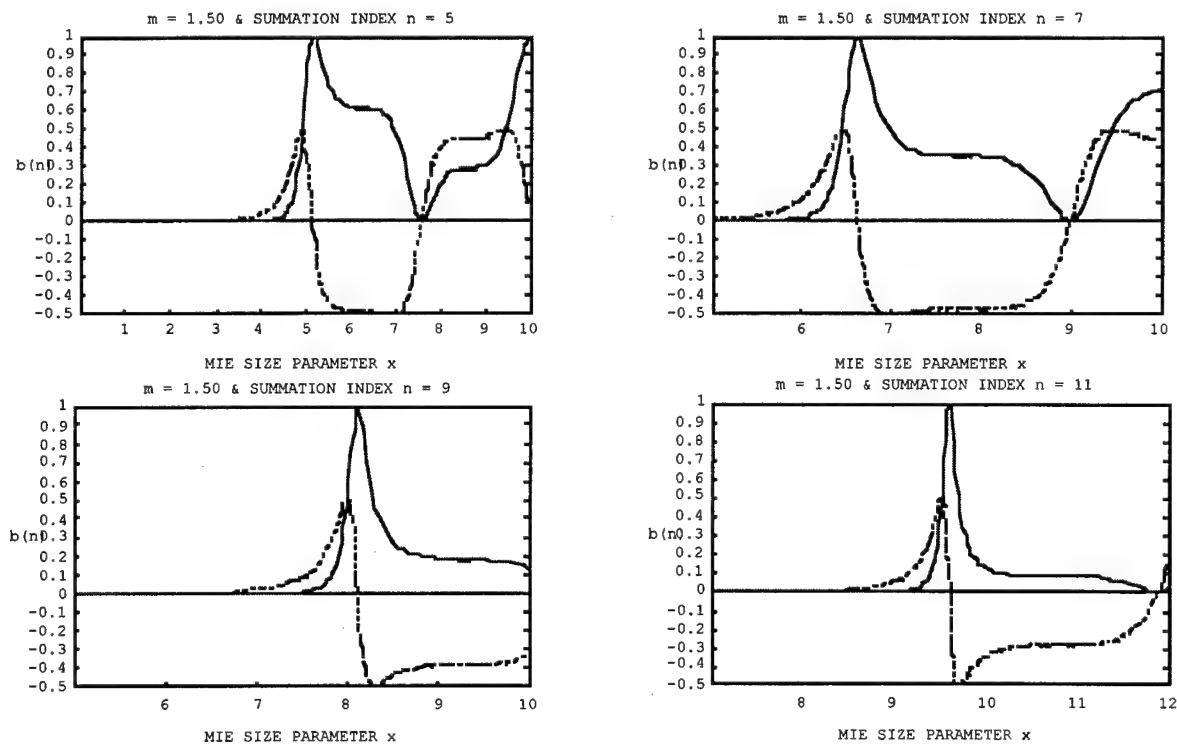
Figure 3-10. Mie calculation of TE-mode component $b_n(x)$ with refractive index $m = 1.50$. *Here the real part and imginary part are plotted in different colors (real part always larger than 0). The first peak in the real part indicates the location of the MDR. The imaginary part determines the width of the given MDR.*

TABLE 3-1. Location and Linewidth for a TE MDR With Mode Number n and Mode Order l in a Microsphere With Refractive Index m.

Mode	Mode No.	Order No.	Resonance Location (x)		Width (FWHM)	
	(n)	(l)	Mie	Approx.	Mie*	Lam
TE	5	1	5.14801	5.02663	2.05723	0.637198
TE	7	1	6.61786	6.6192	0.52115	0.431903
TE	9	1	8.10913	8.16231	0.29716	0.291752
TE	11	1	9.60361	9.67443	0.18515	0.19304

* Resonance width is calculated by the difference in size parameter x where $Im[b_n(x)] = \pm 0.5$.

Then we consider the multiplexing factor functions of the order number of the excited MDR, the refractive index, and the absorption of the microspheres. Since TE-mode MDR is shaper than that of the corresponding TM-mode MDR,[15,16] we will only consider the case of TE-mode operation. The calculation is performed by fixing the central wavelength at 550 nm and allowing the size distribution of microspheres be automatically adjusted for maximizing the multiplexing factor. As expected, the multiplexing factor increases as the size of the microsphere increases (Figure 3-11). The multiplexing factors of low-order MDR's suffer significantly as the absorption factor is included.

3.4 EFFECT OF LATERAL COUPLING

It is well known that the MDR conditions are highly sensitive to the surrounding environment. As the microspheres are set close to each other, the coupling through the evanescent field will increase and thus perturb the properties of the MDR's. This may impose a practical limitation on the packaging density of microspheres on a substrate (see Figure 3-12a) and the capability of tightly stacking the microspheres layers in volume [see Figure 3-12(b)]. This particular information will be considered for a study in system performance projection.

Limited by the scope of this study, we will only present a hand-off argument in judging the effects of lateral coupling. It seems that with proper arrangement the effects of lateral crosstalk in exciting MDR may be minimized. Consider two microspheres in close contact to each other. It is only important for not allowing the central direction (from center-to-center of adjacent microspheres) aligned with the propagation direction of the excitation light.[17] This could be naturally achieved by shifting each closely packed microsphere layer (as illustrated in Figure 3-13). Note that in reality this close-packing arrangement will be very difficult to accomplish. It is especially true when microsphere sizes, selected from a finite size distribution, are not all the same.

46
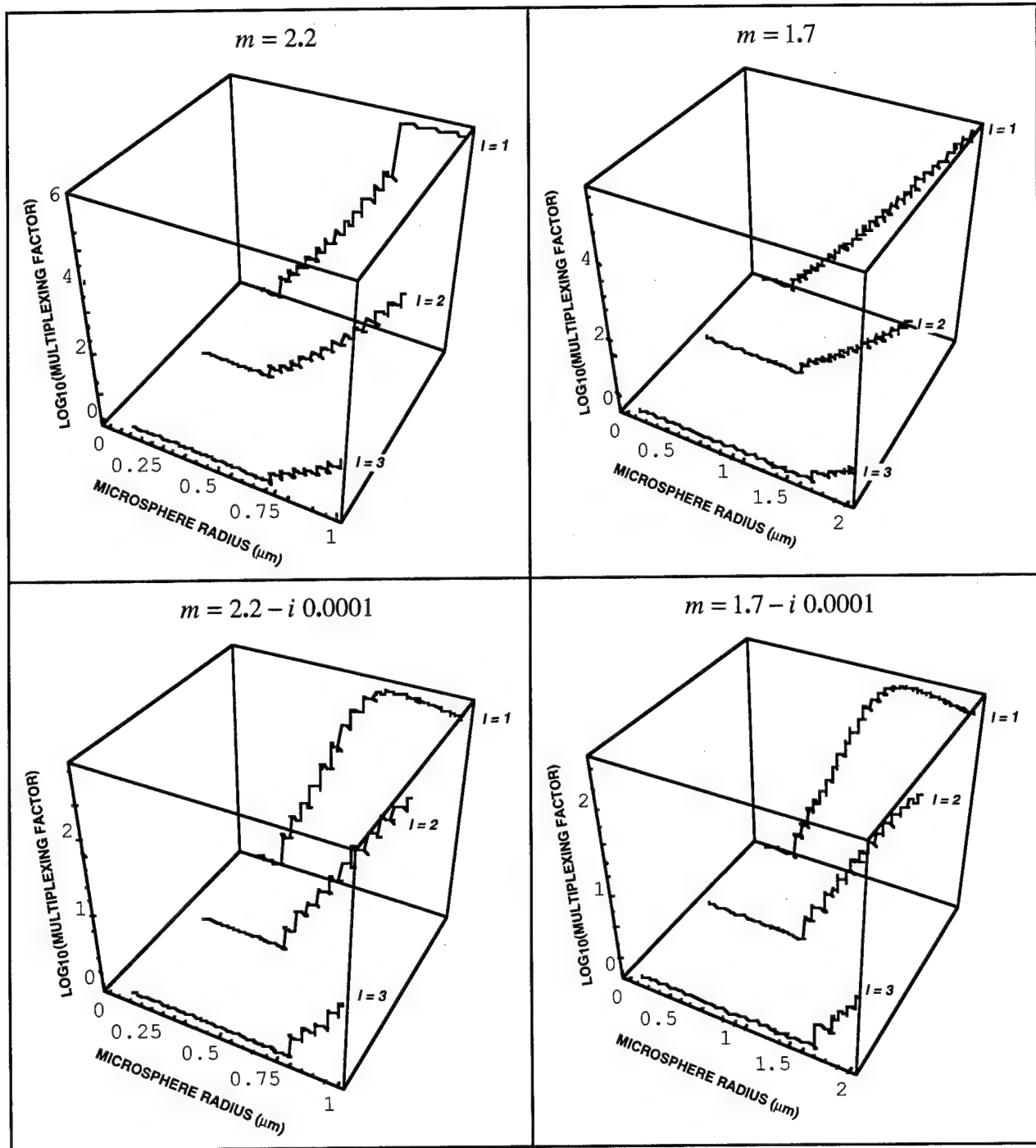
Figure 3-11(a). Multiplexing factor as a function of the microsphere size, order number of the excited MDR, and the complex refractive index of the microsphere. *The medium scanable wavelength is fixed at λ = 550 nm.*

47
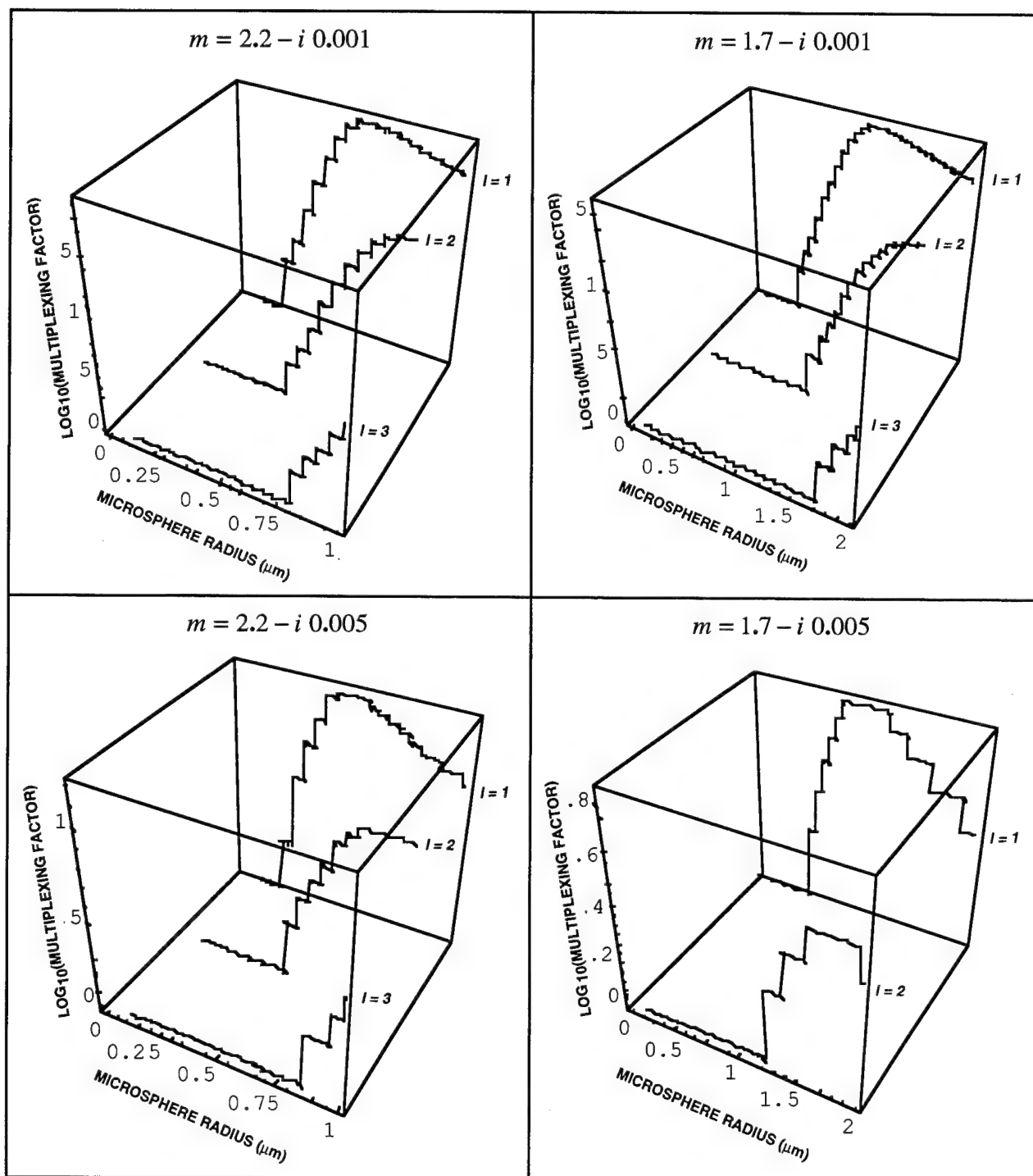
Figure 3-11(b). Multiplexing factor as a function of the microsphere size, order number of the excited MDR, and the complex refractive index of the microspheres.

48
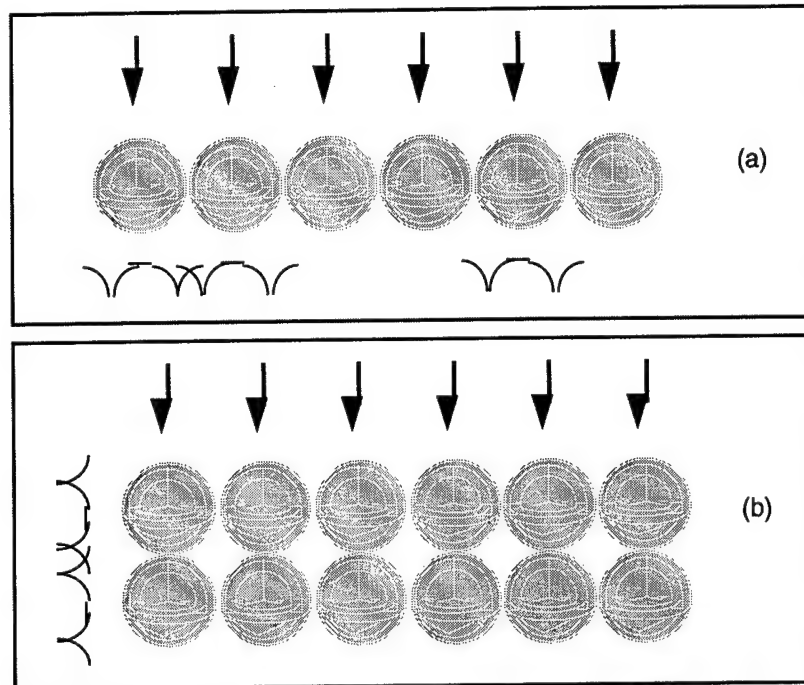
Figure 3-12. Schematic illustrations representing the effects of lateral and vertical optical couplings; (a) lateral optical coupling, (b) vertical optical coupling.

TOP View

EXCITATION

SIDE VIEW
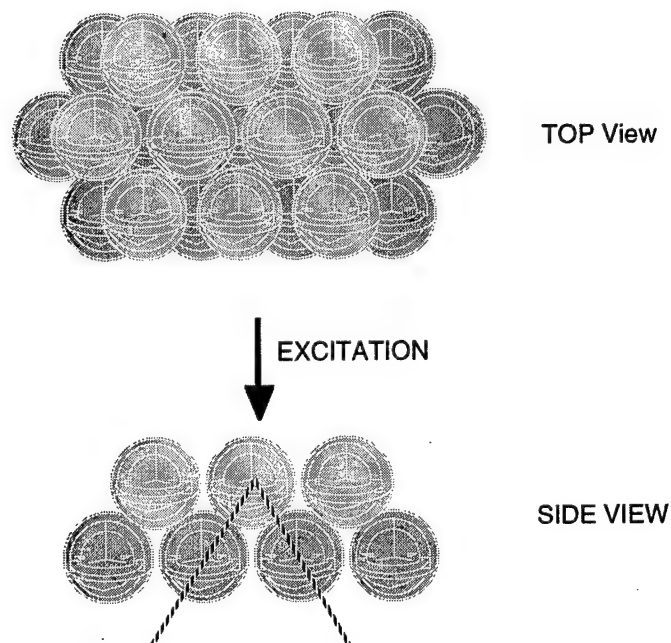
Figure 3-13. Potential crosstalk in exciting MDR may be minimized by avoiding direct contact (between adjacent microspheres) in the direction of line-of-sight.

49

Section 4
SYSTEM ANALYSIS

The first consideration factor for any given data storage technique, especially the 3-D memory system, is the maximization of the data storage density and system storage capacity. In addition, the technology must also optimize several system requirements, such as data transfer rate, signal-to-noise ratio for signal detection, data retention, repeatability of data erasure, and availability of supporting peripherals.[18] Based on the knowledge gained under the tasks of material study and theoretical understanding, we intend to analyze potential performance of the DLMS system.

Data storage density of the room-temperature, MDR-based spectral hole burning depends upon the multiplexing factor that is related to the size of the microsphere distributions. To support a unique, unambiguous MDR in a microsphere distribution with a given nominal size, its size distribution range has to be fairly limited. As a result, the number of allowed frequency channels will be much less than the Q-factor of MDR's. The predicted data storage density is unfortunately low, compared to conventional optical disk technology. In addition, the data transfer rate is largely dominated by the slow spectral hole formation and laser spectral tuning.

Lastly, we review the status of necessary supporting peripherals (such as tunable lasers, spatial light modulators, and imagers) for the DLMS system. In general, those peripherals are common to most high-density 3D memory systems under development. Except for compact tunable lasers, both spatial light modulators (SLMs) and imagers gain leverages from commercial markets in display and electronic imaging. Their fast developments will affect the success of 3D memory systems.

4.1 DLMS SYSTEM PERFORMANCE ANALYSIS

Under this task we first analyzed the most critical factor, the data storage density, for any 3D-based high-density storage system. Factors that determine its data transfer rate and data access time are discussed. Note that the concept-proof system must be significantly improved to make the DLMS-based optical memories practical.

4.1.1 Maximum Storage Density

As described in Section 3, the DLMS allows a reasonable multiplexing factor to microspheres with well-controlled size distribution, although the multiplexing factor is not as large as what we anticipated before. Large multiplexing factor may be achieved in a microsphere distribution with a large averaged size. This is especially true for the low-loss system that possess negligible Q-loss. What important to the system is if the area storage density (bit/μm^2) of the system may outperform conventional optical disks ($\approx$1 bit/μm^2). To make the system worthy for implementation, the

system storage density (# of bits/μm^2) should be at least 10 times higher than conventional optical disk technologies ($\approx$ 1 bit/μm^2). For example, an area density greater than 10 bit/μm^2 has been demonstrated in a photorefractive holographic memory system.[19] With the knowledge of the multiplexing factor available to the system, the upper bound of the data storage area density may be estimated. Here we studied both cases that the microspheres may be assembled in 2-D and in 3-D volume formats.

4.1.1.1 2-D Square Packaging. If all microspheres can be closely packed in a single layer, the areal storage density is given by

$$D_{2D} = \frac{M.F.}{(N \cdot M.F.)(2a)^2} = \frac{1}{N \cdot (2a)^2} \tag{4.1}$$

here N represents the average number of microspheres required to establish a physical wavelength channel.
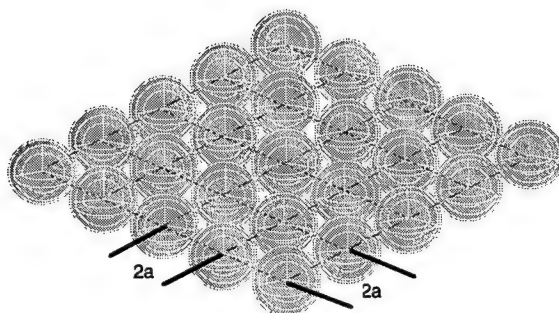
Since at least one microsphere is needed for each channel recording, N must be larger than one. Note that the data storage density for the 2-D packaging scheme is independent of the multiplexing factor. The data storage density of the DLMS is depicted in Figure 4-1. Here we consider the ultimate case of N = 1 and neglect the degradation in multiplexing factor may be caused by the absorption loss. More microspheres (N >>1) are needed to provide signal intensity and S/N ratio. This implies that the realistic data storage density will be much less than what calculated here. If we take the constraints of pixel size ($\approx\lambda^2$) for all optical memory systems, the storage density is worse than what a conventional optical disk can achieve.
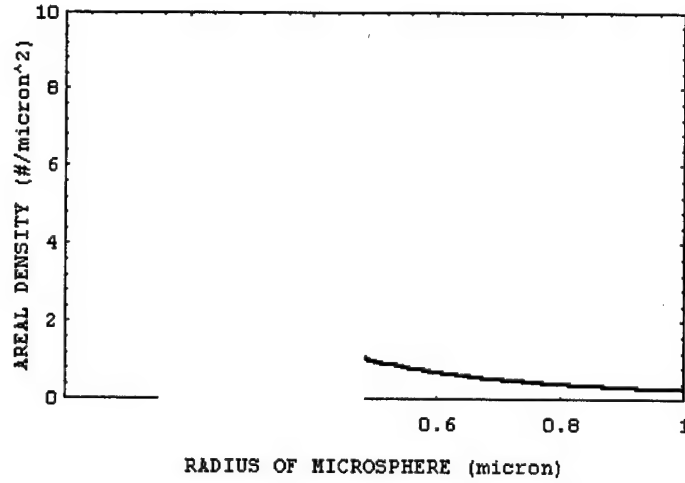
Figure 4-1. Maximum data storage density in the DLMS system. *Here we assume microspheres packed in 2-D format and only one microsphere (N = 1) is needed for each wavelength channel.*

4.1.1.2 Volume Cubic Packaging. In principle the microspheres may be stacked in volume to reduce the footprint of data-storage pixels. In the 3-D packaging case the data storage density may be approximated to be

$$D_{3D} = \frac{M.F.}{(N \cdot M.F.)^{2/3}(2a)^2} = \frac{(M.F.)^{1/3}}{N^{2/3} \cdot (2a)^2}. \tag{4.2}$$

Note that the data storage density of the 3-D packaging scheme will be a function of the multiplexing factor.
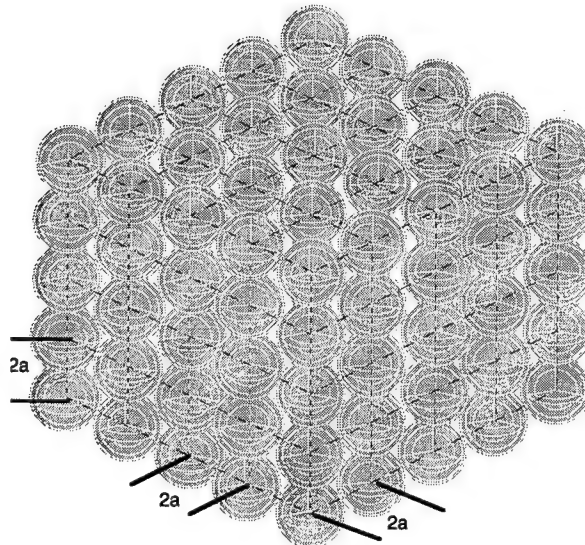
That indicates that the area storage density will be sensitive to the refractive index and the absorption of microspheres. To illustrate the effect of refractive index on the data storage density,

52

we consider two microsphere systems with different refractive indices. The simulation results are shown in Figure 4-2. Again, for simplicity, we assume $N = 1$ and only the lossless systems are considered here. A gain in data storage density may be realized if large-size microspheres are used to achieve large multiplexing factor. Naturally, it also suggests that a large pixel size, on the order of $(N \cdot M.F.)^{2/3}(2a)^2$, is required to accommodate so many microspheres. Unfortunately, it will not be practical to possess any optical memory system with a large 2-D optical aperture.

One potential approach to increase storage capacity with limited pixel area is to develop multilayered storage scheme. The idea is based on IBM's newly developed 3-D optical recording that stacks disk layers together.[20] Each layer will be microspheres packed in volume. Each DLMS layer may be separated by transparent medium and accessed by the using precise dynamic focus control.[21] To enhance signal-to-noise ratio the detection spectrum (for example, fluorescence spectrum of bi-stable dyes) for each individual layer may be tuned to shift away from each other.

Potential effects of optical couplings among compactly packed microspheres is also qualitatively studied.
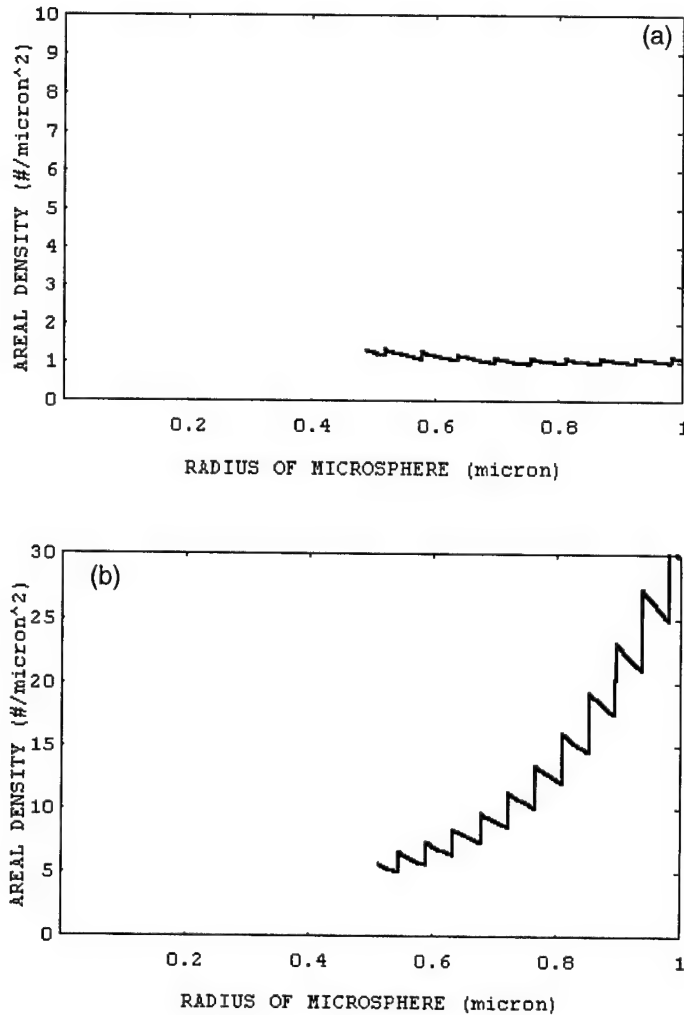
Figure 4-2. Areal data storage density in 3-D volume packaged microspheres: (a) refractive index = 1.7 and (b) refractive index = 2.2. *The average number of microspheres required to establish a physical wavelength channel is assumed to be one.*

4.1.2 Data Transfer Rate

The DLMS-based optical memory system provides parallel accessing capability. Thus, the writing data transfer rate is expected to be determined by the speed of spectral hole formation, tuning rate of the tunable laser, and the frame rate of the SLM. Here the speed of spectral hole formation is fundamentally limited by the writing sensitivity of the dye isomerization. The speed of the read process is expected to be determined by the S/N of the spectral hole-detection (e.g., the fluorescence efficiency of the bi-stable dyes) and the frame rate of the imager. Qualities of encoded spectral holes, both the spectral width and the hole-depth/background ratio, determine the schemes needed for spectral hole-detection. To ensure a proper detection of spectral hole, a multi-point

54

detection scheme may be used to verify the existence of a spectral hole. Unfortunately, such simplicity is gained at expense of slower data transfer rate.

For example, high-speed random-access mass storage is critically needed for improving the database utilization efficiency. Random access and low latency times are synonymous with fast database search. Any new data storage system has to compete with current mass storage technologies, such as 1 Mbytes/s for CD-ROMs, 10 Mbytes/s for magnetic disks, and 1200 Mbyte/s for RAID systems.[19]

The transfer rate of DLMS will be determined by a few factors, such as photoconversion rate, SLM frame rate, and CCD readout rate (in high dynamic range), and overhead of error correction required. In principle, the DLMS was developed for being operated in page mode (data access operates in parallel). Fast transfer speed can be justified for its non-moving storage mechanism. Recent advances in spatial light modulators and multiple-tap CCD imagers all support fast data image transfer. Unfortunately, photoconversion rate of bi-stable dyes dominates the key to faster data transfer rate. In addition, to recognize the existence of a spectral hole, it may require multi-point spectral scanning (as illustrated in Figure 4-3) to verify the existence of a given spectral hole. Although a fast perturbation in wavelength may be achieved electronically, the burden of multiple frame exposure should significantly slow the effective data transfer rate.
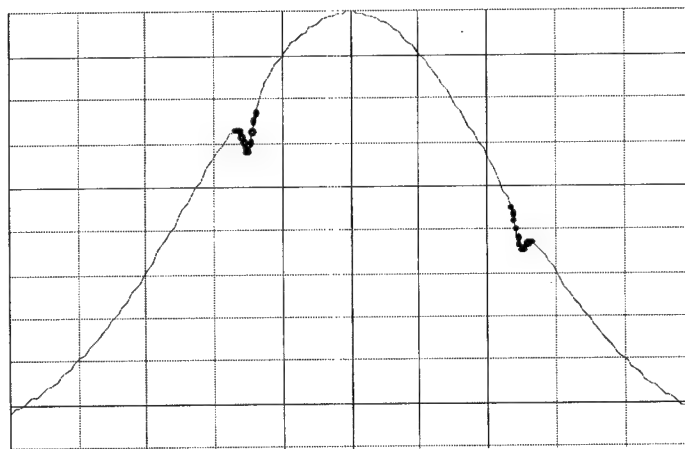
Figure 4-3. Illustration of multi-point scanning for effectively detecting a spectral hole.

4.1.3 Data Access Time

The system access time is determined by a few factors, such as laser wavelength scanning access time, SLM access time, and CCD access time. Since there are no moving parts in SLMs and CCDs and all the information is accessed in parallel, both technologies have potential for rapid data

access. A mechanically tuned laser system will impose a long access time to overall system access time and the effective data transfer rate. It is even more difficult to demand laser wavelength on a random-access basis, in the meantime to maintain wavelength repeatability well within the width of spectral holes to avoid any undesired cross-talk.

4.2 SYSTEM OPERATION ISSUES

4.2.1 Destructive Readout

It is well known that the photochromic recording scheme suffers an important disadvantage that the repeated readouts will significantly degrade the S/N of recorded information.[22] There is a limit to the number of readout may be performed before the S/N drops too low. Note that the internal optical field is non-zero even when the excitation is not matched to the wavelength of the spectral hole. The accumulated destruction will take place for the readout, at any wavelength, is scanned to search for the encoded spectral holes. No reasonable schemes have been found to overcome this difficulty.

4.2.2 Spectral Hole Erasure

Optical erasure capability is essential to the optical data storage devices. For the DLMS-based memory system the erasure can be accomplished by exposing the sample to a UV light source. The UV radiation will activate the returning of the photoproducts to the initial configuration (thus, re-contribute to the fluorescence detection). The main limitations on this subject are the completeness of optical erasure and the inability of selective data erasure. Once data encoded in one wavelength channel are erased, all data encoded in other channels will also be erased. This deficiency will significantly limit its use to be truly "erasable."

4.2.3 Data Recording Conditions

High hole-burning quantum efficiency of bi-stable is desperately needed to ease the laser power requirement and to increase the hole-burning speed. So far all bi-stable dyes tested under this program failed to offer high conversion efficiency. Not only low conversion efficiency demands longer writing time, it also excludes the possibility of writing 2-D information in parallel.

One of the important factors to be considered for all data storage mechanisms is the lifetime of the stored data. Natural thermal activation may push the converted dye back to its original, most stable state. The stability of spectral holes is expected to be determined by the nature of the bi-stable dyes and the dye-microsphere coupling. The experimental results indicate more research efforts are needed in both areas. No significant progress in these areas has been reported.

4.2.4 Channel Integrity

In the theoretical estimation section we assume there is one-to-one correspondence in the frequency channels and the size distribution of microspheres. But, in reality properly placing the "right sizes" of microspheres from a randomly microsphere distribution onto a single pixel is technically challenging, if not impossible. Probability of placing all microsphere in designated sizes onto a single pixel location is fairly low. Missing microspheres or inadequate number of "right size" microspheres will result in missing frequency channels (defects) from the memory area. This is similar to the defects found in disk data technologies. The nature of serial access used in the disk data technologies allows the system to block defects from being accessed. On the other hand, in DLMS the missing frequency channels are randomly distributed in both frequency (ω) and spatial domain (x,y). Parallel 2-D operation requires data flow continuity (e.g., changes in frequency domain) in a given 2-D page pattern. The probability of finding a common multiplexing channel within a 2-D addressable device will be the product of probability of finding that particular channel in all 2-D pixels. It will be impractical to block all defects in both spatial and frequency domains. This presents a significant limitation to address the device in the 2-D parallel format.

Two approaches may be developed to address this issue. First, precision column method may enable us to separate broadly distributed microspheres into microsphere distributions with high precision size control. Batches of precisely selected microsphere size distributions may then be deposited, in sequence, onto the memory pixels. Unfortunately, the challenge of fixing right amounts of given size microspheres in each pixel remains unanswered.

Considering the missing frequency channels as defects, we may apply error correction schemes to guard the integrity of encoded data. To improve data reliability, an error-correction coding schemes have been commonly used to store and retrieve data in the system. Error correction schemes have been proposed to page-mode operation.[23-25] Here error correcting systems add "redundant" information (in 2-D format) to guard the information. If the added structure information is altered by errors (e.g., the missing channels), the changes may be detected. As long as the number of errors is within the correction capability of the error correcting code, the errors caused by the defects may be properly corrected.

4.3 ASSESSMENT OF CRITICAL COMPONENT TECHNOLOGIES

The DLMS memory operations rely on a spatial light modulator to properly encode the optical writing beam, a tunable laser source to reference the frequency channel, an imaging array to detect and convert the optical readout beam into electronic information, and supporting electronics to perform data management. Among them the high-capacity, high speed SLMs and high-resolution, fast frame rate imagers are common to most 3-D memory systems currently under development. Thanks to common interests in display and imaging markets, both SLMs and imaging arrays have

advanced rapidly. Both key components would gain further performance improvements as commercial display and imaging markets continuously push technologies ahead. Compact laser sources, especially semiconductor and/or solid state lasers, have also attracted tremendous commercial interest and gained respectable advances. Although tunable semiconductor lasers have advanced fast, the development of lasers with high fast tuning rate and wide tuning range is lagging behind the other key components.

4.3.1 Imager Arrays

The "Work Horse" of the imager industry is still the Charged-Coupled-Device (CCD) Imager technology, with typical array sizes of 500 to 1000 elements per linear side for consumer needs. However, there are devices for special applications (e.g., surveillance) having array sizes in excess of 5,000×5,000 elements (Loral, Dalsa, and Philips).

The typical dynamic range of these devices (See Table 4-1) is 50-70 dB with room temperature operation. This should be adequate for the DLMS optical memory applications.

The main issue with this technology as it stands now is the frame rate or imaging speed which is typically that of a video 60 Hz rate. This falls significantly short of reading speeds needed. Thus, a reading speed of 1 GHz would imply a frame rate of 1 KHz for a 1,000×1,000 pixel device. A typical ADC (Analog-to-Digital Converter) used in tapping out the data from the CCD device would have a sampling rate of 10 to 20 MHz (for 8-bit resolution). It follows that one would need at least a 50-Tap readout circuitry which while possible, is not very practical.

An old imager concept in a new design has recently emerged. This is a class of imagers called CMOS Sensors which are based on MOS photodiode with a buffer amplifier at each pixel with a column-by-column readout of the information typically into an ADC circuit. Some of the main companies manufacturing this type of sensors are: VVL (UK); IMEC (Belgium), Photobit (CA, USA), and IVP (Sweden). The main advantages of this class of imagers are their being fully compatible with CMOS fabrication and foundry requirements. This is in contrast to the CCD devices which are generally not compatible with the CMOS fabrication constraints. This means that the fast shrinking trend of the minimum feature design rule (presently at the 0.5 to 0.35 μm level) can be followed. This, in turn, means a significant cost advantage due to the increased number of devices which can be produced from each fabricated wafer.

From the Optical Memory standpoint, the advantage of this structure is in the capability of extracting only regions-of-interest which can be selected "on the fly" without the need to readout the whole array. The potentially small feature size would imply faster devices and hence faster multiplexing and readout. Thus this technology is expected to be a better solution for Optical Memory from the stand point of readout speed as well as cost.

Table 4-1. Representative CCD Imagers.

Manufacturer	Technology	Model #	Array Size	Dynamic Range (dB)	Frame Rate (Hz)	Pixel Size (μm)
Kodak	CCD(2-phase)	KAF-6300	3072×2048	72	30	9×9
EG&G Reticon	CCD(3-phase)	RA1101J	1024×1024	77	30	13.5×.3.5
Loral	CCD		2048×2048	80		15×15
Sony	CCD		756×581			
Pulnix	CCD	TMC 9700	768×484	50	30	11.6×13.6
NEC	CCD	NC-832	750×500 (?)	62	30	
Philips	CCD	FT-CCD	720×580	Est. 72	50	6.0×12.6
Dalsa	CCD	IA-D2	512×512	68 (ModelIA-D1)	30	10×10
Sanyo	CCD	LC9931	378×240	66 (12 bit)	30	12.7×15
Thomson-CSF	CCD	7895-A	512×512	72	50-100	19×19
SITe	CCD	S1502A	512×512	90(@-45°C)	5-10	24×24
Electrim(TI)	CCD	EDC1000	753×488	63	30	11.5×27

4.3.2 Spatial Light Modulators (SLMs)

The classes of Spatial Light Modulators which should be considered for the Optical Memory application are Liquid Crystal based Devices, Multiple Quantum Well (MQW) Devices, Electro-Mechanical Devices (Deformable Mirror), and Magneto-Optical (MO) Devices. Other devices such as Acousto-Optical or PLZT-based modulators will probably not be practical candidates. The Acousto-Optical is inherently a one dimensional device and the use of two orthogonal devices even though possible, will result in a significant complexity of the system. The PLZT-based SLMs are not mature enough and suffer from the need of a high driving voltage limiting the minimum pixel size attainable.

The Magneto Optical Device and the Multiple quantum well devices are also not deemed to be suitable for the Optical Memory application. The MO device has (a) a limited production; (b) its optical transmission is low and limited to the yellow-red portion of the spectrum. The quantum well device, while being the fastest SLM (100 KHz operation recently demonstrated) is not practical due to (a) its extremely narrow spectral range and (b) its low optical modulation efficiency.

This leaves the liquid crystal devices and the deformable mirror SLM as the only practical choices for this application. The deformable mirror Device is at least presently a good choice for our application as it is a mature device technology. It also has the technical advantages of being

broad-band and, not requiring polarized light—with the added system simplicity and optical throughput. For binary-mode operation it can run at frame rates of about 10 KHz. For Gray-scale operation it is reduced (depending on the contrast resolution required) to below 1 KHz. This is still quite sufficient to get us the required ~GHz writing throughputs, assuming a 1000×1000 pixel page size.

However, for future systems requiring up to THz throughputs, this technology will be limited in its frame rate capability due to mechanical resonances. A Ferroelectric or Deformable-Helix type Smectic LC modulators may provide the needed ~1 MHz frame rate, but with penalties of either low optical modulation throughput (DHL) and effective narrow band operation. The latter term refers to the fact that while both devices can operate over a wide spectral range, they will require different setting for each wavelength band due to its controlled-birefringence operation (i.e., the bias voltage will have to be switched for each wavelength. This however may still be practically realizable (albeit more complex).

Finally, the Nematic class of LC modulator, while potentially providing broadband operation, is inherently too slow <1 KHz for the Optical Memory application.

4.3.3 Compact Tunable Laser Source

To accomplish the wavelength multiplexing operation, the system demands a tunable laser capable of fast and agile spectral tunability. The tunable spectral range should be as wide as possible and well matched to the characteristics of the bi-stable dyes used in the system. The spectral width of the laser source should closely match to the width of the spectral holes. Important factors also include wavelength stability (either short-term and long-term stability), wavelength tuning repeatability, and the tuning speed. Tuning repeatability is a measure of the accuracy to which the laser is randomly tuned. To ensure proper channel registration, the wavelength tuning repeatability should not exceed 1/2 of the expected width of spectral holes. In addition, the ideal tunable laser should also provide high power and self-attenuation capability for allowing fast switching between writing and readout modes.

Dye lasers, vibronic solid-state tunable lasers (e.g., Ti:sapphire laser),[26] optical parametric lasers[27] and current-tuned and thermal-tuned semiconductor lasers are all capable for wide range wavelength tunability. Among them the dye laser is the most mature technology and the spectrum range can be optimally matched by choosing proper dyes. Spectral tuning repeatability represents a common weak point for all tunable lasers. For example, the AUTOSCAN II system from Coherent Laser has a specified absolute accuracy of ±200 MHz and reproducibility of ±50 MHz. The absolute wavelength accuracy and its reproducibility are much large than its linewidth. That simply impose a limitation on how narrow the encoded spectral holes can be. Note that the width of

spectral holes must be about the maximum of those uncertainties to ensure proper channel registration.

As discussed previously the tuning speed of the tunable laser can be a dominating factor to the overall data access time. The wavelength selection is achieved by employing wavelength-selected cavity optics.[28] High speed fine frequency tuning can be achieved by electro-optic methods. Unfortunately, the tuning ranges are generally quite limited. For wider range tunability it is necessary to use mechanical tuning scheme for wavelength selection.[29] Mechanical tuning mechanisms, such as diffraction grating, birefringent plate, and tuning prism, are especially needed for coarse wavelength selection across the entire tuning range. As expected, mechanical tuning imposes serious limitations on the tuning speed and the wavelength repeatability. This procedure can be very slow and take up to a few seconds.

Although dye lasers are technology-matured and commercially available, the systems are generally large-size and require constant maintenance. The development of solid dye laser system will also ease some maintenance trouble,[30] but they are still far from being user friendly. When system implementation factors (e.g., compactness, ruggedness, reliability, and uncomplicated handling) are considered, a semiconductor laser diode is the ideal excitation source. The ideal, compact tunable laser system is far from mature and more research study is required.

4.3.4 Electronics and data processing

To manage a high-capacity data storage system requires sophisticated electronics and algorithms to efficiently transfer, store, and encode data. Recently this issue has started attracting researchers' attention. A typical example is the use of MUISC (Multi processor System with Intelligent Communication), a single instruction multiple data (SIMD) parallel processor system for managing spectral hole-burning-based holographic memory system.[31] Since the system is designed for 2-D page-mode operation, we should try to process data directly in optical domain and fully utilize the parallel processing capability. An all-optics, or a quasi-parallel, processing unit should be introduced into the system to speed up data processing.

Section 5
REFERENCES

1. P. Chylek, J.D. Pendleton, and R.G. Pinnick, "Internal and near-surface scattering field of a spherical particle at resonant conditions," Appl. Opt. **24**, 3940 (1985).

2. P.W. Barber, S.C. Hill, *Light scattering by particles: computation methods,* Advanced series in applied physics, Vol. 2 (World Scientific, Singapore, 1990).

3. W.J. Wiscombe, "Improved Mie scattering algorithms," Appl. Opt. **19**, 1505 (1980).

4. H.B. Lin, A. L. Huston, J. D. Eversole, A.J. Campillo, and P. Chylek, "Internal scattering effects on microdroplet resonant emission structure," Opt. Lett. **17**, 970 (1992).

5. H.S. Bennett and G.J. Rosasco, "Resonances in the efficiency factors for absorption: Mie scattering theory", Appl. Opt. **17**, 491 (1978).

6. R.K. Johnson, "Morphology-dependent resonances of a dielectric sphere on a conducting plane," J. Opt. Soc. Am. A **11**, 2055 (1994).

7. T. Kaiser and G. Schweiger, Computers in Phys. **7**, 682 (1993).

8. M. Kerker, *The scattering of light and other electromagnetic radiation* (Academic, New York, 1969).

9. A.B. Pluchino, "Surface waves and the radiative properties of micron-sized particles," Appl. Opt. **20**, 2986 (1981).

10. R. Bhandari, "Scattering coefficients for a multilayered sphere: analytic expressions and algorithms," Appl. Opt. **24**, 1960 (1985).

11. R.L. Hightower and C.B. Richardson, "Resonant Mie scattering from a layered sphere," Appl. Opt. **27**, 4850 (1988).

12. J.A. Lock, "Interference enhancement of the internal fields at structural scattering resonances of a coated sphere," Appl. Opt. **29**, 3180 (1990).

13. K.A. Fuller, "Scattering of light by coated spheres," Opt. Lett. **18**, 257 (1993).

14. C.C. Lam, P.T. Leung, and K. Young, "Explicit asymptotic formulas for the positions, widths, and strengths of resonances in Mie scattering," J. opt. Soc. Am. B **9**, 1585 (1992).

15. G.J. Rossasco and H. S. Bennett, "Internal field resonance structure: Implications for optical absorptio and scattering by microscopic particles," J. Opt. Soc. Am., Vol. 68, 1242 (1978).

16. H.B. Lin, A.L. Huston, B. L. Justus, and A.J. Campillo, "Some characteristics of a droplet whispering-gallery-mode laser," Opt. Lett. **11**, 614 (1986).

17. S. Arnold, J. Comunale, W.B. Whitten, J.M. Ramsey, and K.A. Fuller, "Room-temperature microparticles-based persistent hole-burning spectroscopy," J. Opt. Soc. Am. B **9**, 819 (193).

18. B.D. Terris, et al., Appl. Phys. Lett. **68**, 141 (1996)

19. J.H. Hong and D. Psaltis, "Dense holographic storage promise fast access," Laser Focus World, 119, April 1996.

20. T. Tanaka and S. Kawata, JOSA A **13**, 935 (1996)

21. K. Osato and G. S. Kino, "Electro-optic focusing for a high-density optical disk," Opt. Lett. **18**, 1244 (1993).

22. T. Tsujioka, F. Tatezono, T. Harada, K. Kuroki, and M. Irie, "Recording sensitivity and superlow-power readout of photon-mode photochromic memory," Jpn. J. Appl. Phys. **33**, 5788 (1994)

23. H.J. Mamin, B.D. Terris, L.S. Fan, S. Hoen, R.C. Barrett, D. Rugar, IBM J. Res. Develop. **39**, 681 (1995)

24. A.A. Neifeld and M. McDonald, "Error correction for increasing the usable capacity of photorefractive memories," Opt. Lett. **19**, 1483 (1994).

25. M.A. Neifeld and J.D. Hayes, "Error-correction schemes for volume optical memories," Appl. Opt. **34**, 8183 (1995)

26. P F. Moulton, "Tunable solid-state lasers," Proc. IEEE **80**, 348 (1992).

27. M.J. Padgett and M. H. Dunn, "Dye-laser alternatives cover the spectrum," Laser Focus World, 69, **September** 1994.

28. T.V. Higgins, "The three phases of lasers: solid-state, gas, and liquid," Laser Focus World, 73, **July** 1995.

29. B. Maisenbacher, E. Leckel, R. Jahn, and M. Pott, "Tunable laser sources for optical amplifier testing," HP Journal, 11, Feburary 1993.

30. A. Costela, I. Garcia-Moreno, J. M. Figuera, F. Amat-Guerri, and R. Sastre, "Solid-state dye lasers based on polymers incorporating covalently bonded modified rhodamine 6G," Appl. Phys. Lett. **68**, 593 (1996).

31. W. Graff, A. Rosselet, U.P. Wild, R. Gschwind, and C.U. Keller, "Handling of huge multispectral image data volumes from a spectral hole burning devices (SHBD)," SPIE **2480**, 445 (1995).

MISSION
OF
ROME LABORATORY

Mission. The mission of Rome Laboratory is to advance the science and technologies of command, control, communications and intelligence and to transition them into systems to meet customer needs. To achieve this, Rome Lab:

    a. Conducts vigorous research, development and test programs in all applicable technologies;

    b. Transitions technology to current and future systems to improve operational capability, readiness, and supportability;

    c. Provides a full range of technical support to Air Force Material Command product centers and other Air Force organizations;

    d. Promotes transfer of technology to the private sector;

    e. Maintains leading edge technological expertise in the areas of surveillance, communications, command and control, intelligence, reliability science, electro-magnetic technology, photonics, signal processing, and computational science.

The thrust areas of technical competence include: Surveillance, Communications, Command and Control, Intelligence, Signal Processing, Computer Science and Technology, Electromagnetic Technology, Photonics and Reliability Sciences.